materials

MDPI

Review

An Overview of Photocatalytic Membrane Degradation Development

Mojtaba Binazadeh [1], Jamal Rasouli [1], Samad Sabbaghi [2,*], Seyyed Mojtaba Mousavi [3], Seyyed Alireza Hashemi [4] and Chin Wei Lai [5,*]

[1] Department of Chemical Engineering, School of Chemical and Petroleum Engineering, Shiraz University, Shiraz 71557-13876, Iran; binazadeh@shirazu.ac.ir or binazade@ualberta.ca (M.B.)
[2] Department of Nano-Chemical Engineering, Faculty of Advanced Technologies, Shiraz University, Shiraz 71557-13876, Iran
[3] Department of Chemical Engineering, National Taiwan University of Science and Technology, Taipei City 106335, Taiwan
[4] Nanomaterials and Polymer Nanocomposites Laboratory, School of Engineering, University of British Columbia, Kelowna, BC V1V 1V7, Canada
[5] Nanotechnology & Catalysis Research Centre, University Malaya, Kuala Lumpur 50603, Malaysia
* Correspondence: sabbaghi@shirazu.ac.ir (S.S.); cwlai@um.edu.my (C.W.L.)

Abstract: Environmental pollution has become a worldwide issue. Rapid industrial and agricultural practices have increased organic contaminants in water supplies. Hence, many strategies have been developed to address this concern. In order to supply clean water for various applications, high-performance treatment technology is required to effectively remove organic and inorganic contaminants. Utilizing photocatalytic membrane reactors (PMRs) has shown promise as a viable alternative process in the water and wastewater industry due to its efficiency, low cost, simplicity, and low environmental impact. PMRs are commonly categorized into two main categories: those with the photocatalyst suspended in solution and those with the photocatalyst immobilized in/on a membrane. Herein, the working and fouling mechanisms in PMRs membranes are investigated; the interplay of fouling and photocatalytic activity and the development of fouling prevention strategies are elucidated; and the significance of photocatalysis in membrane fouling mechanisms such as pore plugging and cake layering is thoroughly explored.

Keywords: photocatalytic membrane reactor; membrane; nano photocatalyst; drinking water treatment

check for updates

Citation: Binazadeh, M.; Rasouli, J.; Sabbaghi, S.; Mousavi, S.M.; Hashemi, S.A.; Lai, C.W. An Overview of Photocatalytic Membrane Degradation Development. *Materials* **2023**, *16*, 3526. https://doi.org/10.3390/ma16093526

Academic Editors: Andrea Petrella and Enrique Fernandez Ledesma

Received: 3 February 2023
Revised: 9 March 2023
Accepted: 27 March 2023
Published: 4 May 2023

Copyright: © 2023 by the authors. Licensee MDPI, Basel, Switzerland. This article is an open access article distributed under the terms and conditions of the Creative Commons Attribution (CC BY) license (https://creativecommons.org/licenses/by/4.0/).

1. Introduction

Industrial organic pollutants such as hormones, pesticides, pharmaceutically active substances, and personal care products have become a growing environmental concern due to their continuous release into the waterways and subsequent detrimental effects on human health, plants, soil, and aquatic systems [1–4]. Over a long period, antibiotics in their active form (low doses) and their main components can alter microbial communities in bodies of water [5,6]. Studying water samples of wastewater treatment plants in Beijing, China, revealed high concentrations of tetracycline, sulfonamides, and quinolones [7].

To remove contaminants and lessen their adverse effects on the environment and human health, a number of purification approaches are available, such as chemical coagulation [8], biodegradation [9], flotation [10,11], absorption [12], and adsorption [13]. Despite their benefits, conventional procedures have drawbacks, such as their inability to entirely remove contaminants. For instance, there are a number of drawbacks to the adsorption technique used for wastewater treatment, such as the challenging nature of separating the adsorbent from the solution and the high cost of the adsorbent [14,15]. Therefore, it is crucial to develop a novel, incredibly efficient method to eliminate contaminants from wastewater before they enter the environment [16].

The development of innovative green chemical technologies and methods in organic synthesis and environmental converters has emerged as one of the most pressing topics for chemical researchers in recent decades, particularly those working with heterogeneous photocatalysis (HPC). Too much emphasis is placed on exploiting the sun as a renewable energy source, and visible light photocatalysts play a critical role in this regard [17,18]. Progress in photocatalysis, an improved oxidation process, has been rapid in recent years. This technology has gained a reputation for being sustainable and efficient at reducing energy use and harming the environment [19,20]. The membrane separation process is also one of the most common and widely used methods for treating contaminated water. Membrane technology is simple to operate, requires little space, and allows product recovery at high efficiency and high selectivity. Membrane separation is done at normal operating temperatures and does not require phase change [21,22]. Membranes are classified into different types depending on the material, structure, geometry, manufacturing method, and type of process used. Organic, inorganic, and composite materials may be used for production of flat, hollow fiber, or tubular membranes [23–26]. Based on the substance employed, membrane production is primarily divided into organic (polymeric) and inorganic membranes [27,28]. Inorganic membranes are those that incorporate metals, oxides, or elementary carbon in their structure, such as zeolite, ceramic, and metallic membranes, while organic membranes are those constructed of nonporous polymeric materials, including polyethersulfone, polysulfone, polymethylpentene, cellulose acetate, polycarbonate, polyimide, polyetherimide, polydimethylsiloxane, and polyphenylene oxide [27,29,30]. The separation techniques used in these systems are usually vacuumed filtration or pressure filtration using microfiltration, ultrafiltration, or nanofiltration membranes [31,32]. Polymeric synthetic membranes make up a sizable portion of industrial membranes. Compared to mineral membranes, these membranes are more commonly used because as they are easier to build, less expensive, and more processable [33].

Combining photocatalysis and membrane filtration is a widely used method that can be effective for the removal various contaminants from the aqueous system. Therefore, the design and development of photocatalytic membrane reactors (PMRs) have become a popular and effective method for treating polluted water. The number of articles published annually on PMRs is depicted in Figure 1. PMRs differs from conventional photocatalytic reactors as the photocatalyst remains in the system and treated water selectively permeates through the membrane. PMRs enhance process efficiency, controllability, and stability. They also minimize installation space, energy requirement, and eliminate extra expenditures associated with flocculation, coagulation, and sedimentation [34,35]. The photocatalyst in the PMR system can photodegrade pollutant molecules stuck to the membrane surface using visible light, sunshine energy, and UV radiation [36].

Both polymeric and mineral membranes have shown excellent self-cleaning and anti-fouling properties through photodegradation when exposed to visible light and UV irradiation [37,38]. A photocatalytic membrane may utilize the absorbed energy from the irradiation source and breaks down pollutants that adhere to its surface; thus, such a membrane is self-cleaning and anti-fouling [38].

The main focus of this research is how to use PMRs to clean water and waste water. The photocatalyst, membrane, and light source are the main components of PMRs that are hereby discussed in depth. Membrane fouling is a serious operational concern in slurry-type reactors; thus, its effects on permeate flux and system efficiency are described in length, along with solutions for mitigating the impacts of membrane fouling. Several of the most crucial operational variables that affect PMRs performance are covered. The standards for creating and developing PMRs are provided. Lastly, the most recent developments in the utilization of visible light are also discussed, along with efforts to circumvent some of the inherent drawbacks of PMRs, such as a moderate loss of photoactivity, constrained processing speeds due to mass transfer issues, membrane leakage, and unsatisfactory system lifetimes due to photocatalyst leaching.

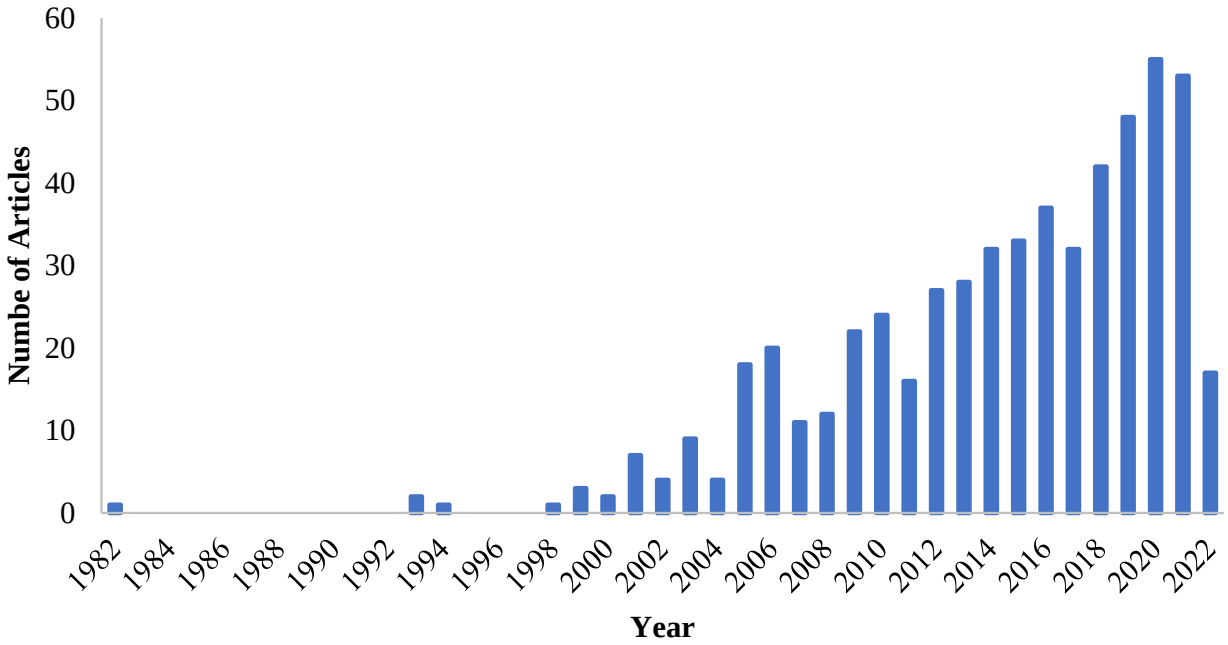


Figure 1. The number of articles published annually on the topic of photocatalytic membrane reactors based on Scopus (searched "Photocatalytic membrane reactor").

2. Mechanism of Photocatalysis and Membrane Processes

2.1. Photocatalytic Degradation Mechanism

As schematically shown in Figure 2a, degradation reactions are driven by the electrons transferred from the valence to the conduction band. Typically, a photocatalyst's band-gap energy (E_a) should be equal to or less than the emitted photon energy [39–41]. Electron transfer results in formation of an associated hole (h^+_{VB}) in the valence band [42,43]. Electron-hole pairs promote both oxidation and reduction of the adsorbed layer by generation of radicals [17,44]. Radicals are active oxidizing and reducing species that attack to and degrade contaminants in the aqueous solution [45,46]. A substrate reduction potential below that of hole (h^+_{VB}) results in the oxidation of substrates in the valence band, whereas a substrate reduction potential higher than that of electron (e^-_{CB}) results in the reduction of substrates in the conduction band [47,48]. Hydroxyl radicals (•OH) are the main species responsible for the photodegradation of pollutants. Another oxidant is reactive oxygen species (ROS), such as superoxide oxygen radicals ($O_2^{\bullet -}$) [47]. Figure 2b shows photocatalytic degradation of cefixime, as an example of pharmaceutical pollutants, by Fe_2O_3@TiO_2 [13].

2.2. Mechanism of the Membrane Filtration Process

Pressure, concentration, or electric potential differences are the driving forces of membrane separation techniques. PMRs operate by pressure and concentration differences. Generally, surface water recycling for non-drinking purposes involves the utilization of ultrafiltration (UF) and microfiltration (MF) membranes. Nanofiltration membranes (NF) with molecular weight cut-offs (MWCO) between 150 and 350 Da are suitable for wastewater treatment and environmental cleanups due to their excellent inorganic ion removal capabilities [21].

The contaminated feed solution passes through the membrane under pressure. Membrane in a PMR retains the photocatalyst and pollutants and preferentially permeates water [49–51] as depicted in Figure 3a. In photocatalysis conditions at PMRs, polymeris membranes are highly susceptible to (1) abrasion by the photocatalyst and (2) degradation assisted by hydroxyl radicals. Thus, inorganic membranes are preferable due to their superior chemical, mechanical, and thermal resistance. One drawback of inorganic membranes is their cost. A thinner membrane enhances permeate flux due to its lower hydraulic

resistance. However, if the membrane is too thin, it may be vulnerable to damage. Average pore size diameter, chemical, mechanical and thermal stability, cost, and lifetime are other important parameters that must be tailored for each membrane application. A list of membranes used for water decontamination is reported in Table 1.

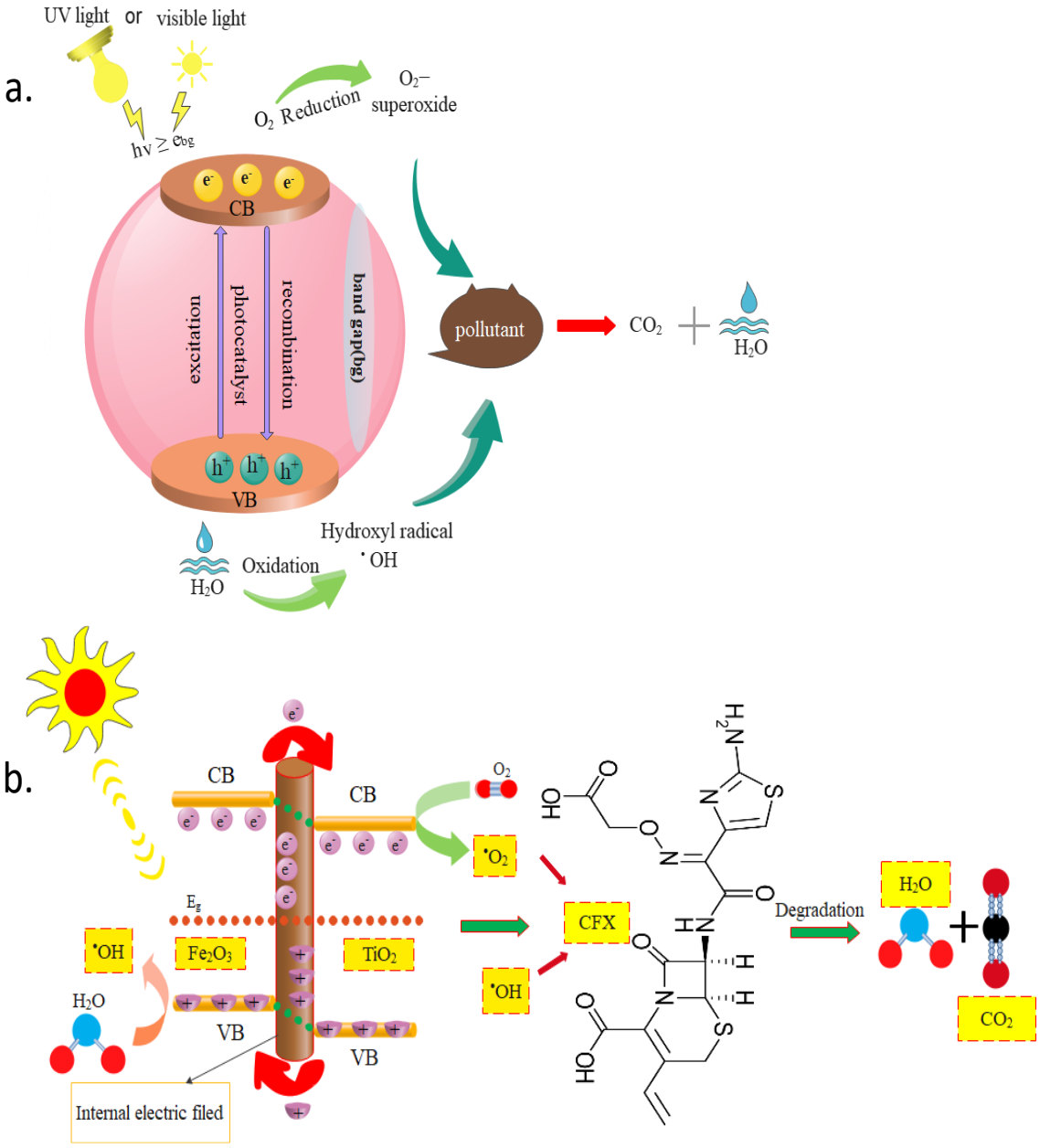


Figure 2. (**a**) Mechanism of photocatalytic degradation of pollutants, and (**b**) mechanism of cefixime photocatalytic degradation via Fe_2O_3@TiO_2 photocatalyst [13]. Adapted with permission from Elsevier. Copyright 2023.

Table 1. Membranes for water decontamination.

Membrane	Material	Manufacturer	Thickness (mm)	Pore Size (μm)	P (bar)	T (K)	Pollutant	Membrane Separation (%)	Ref.
Commercial spiral wound polyamide nano filter	TFC	-	-	-	8	-	COD	98	[52]
AGS reactor, UP and NF	PES, PESH, and PA	-	-		0.5	293.15	COD	51.33, 90.48 and 99.26	[53]
Hollow fiber UF membrane	PVC	-	0.185	0.01–0.1	1	298.15	methyl green dye (MG)	94.79	[54]
NF membrane	piperazine based polyamide, proprietary (cross-linked modified polyacrylonitrile), polyethersulfone	Toray chemical, Koch membrane systems, Nadir	-	0.1	30	-	copper-refining sulfuric acid wastewater	95	[55]
A sheet nano-porous membrane	PAN	Sepro Membranes of USA.	Top layer 0.1–0.5 and Sublayer 100–150	0.01	4	318.15	TSS, TDS, content of oil and grease, COD and BOD5	100, 44.4, 99.9, 80.3 and 76.9	[56]
Multichannel tubular	Ceramic membrane	Jiangsu Jiuwu HiTech Co. Ltd., Nanjing, China		0.05	2	233.15	suspended solid, turbidity, and total phosphorus	100, 99.20, and 80.21,	[57]
SW30 membrane BW30 NF270	PA	-	-	-	69 41 41	318.15	COD and TPh	(95.18, 91.15, 80.11) and (98.02, 96.06, 27.08)	[58]
Difluoride hollow fiber membrane module	PVDF	M/s. TECHNIC, India	-	0.1	0.5–1	-	TOC	64	[59]

As depicted in Figure 3 there are four main solute transfer mechanisms in membranes. The main transport mechanism for a membrane process is determined by relative magnitude of (1) average pore size diameter (d), (2) size difference of transferable and nontransferable molecules, (3) mean free path of transferable molecule (λ), and (4) pore network structure. According to Figure 3b, presence of large pores in the membrane ($d/\lambda > 20$) results in convective flux. Convective flux through membrane accelerates the process; however, convection mechanism is only applicable in PMRs when there is a large size difference between contaminants/photocatalyst and water molecules. If such size difference does not exist, membranes with smaller pore size are required which transport water molecules by permeation. The permeation rate is affected by various factors, including pressure and concentration gradient, size and shape of permeate, and pore size, thickness and chemical structure of membrane. There are two main forces that drive the permeation: hydraulic pressure, which pushes solvent molecules through the membrane, and osmotic pressure, which opposes the flow of solvent due to the presence of dissolved species in the wastewater [60]. The Knudsen diffusion mechanism is dominant when $d/\lambda < 0.2$ [61]. Knudsen diffusion occurs only during gas transfer across nano porous membrane; thus, it is useful in removing gases and volatile organic compounds from wastewater [62,63]. Molecular sieves may also be used to purify water [64]. Solution–diffusion is the main transport in dense membranes. Solution–diffusion does not apply to water purification; however, it is the main mechanism for hydrogen transport in Pd-based membranes [65].

During the filtration process, pollutants adhere to the membrane surface and decrease membrane permeability. This phenomenon is calling membrane fouling which is one of the most important challenges of membrane processes [66,67].

Adsorption, accumulation, and precipitation are three mechanisms that may simultaneously occur to produce fouling [68,69]. To improve membrane performance, its surface is modified to maximize its affinity towards the permeating solvent and minimize its affinity towards the fouling agents [70]. Chemical modification, UV irradiation, applied electric field, aeration, and plasma treatment may be utilized to tune hydrophilicity of the

membrane surface [71]. Filtration at critical flux has a modest flux drop and minimized irreversible fouling; however, it reduces output. Finally, to maintain the performance of the membrane system, cleaning and maintenance strategies such as backwashing and chemical cleaning are employed routinely during operation [72,73].

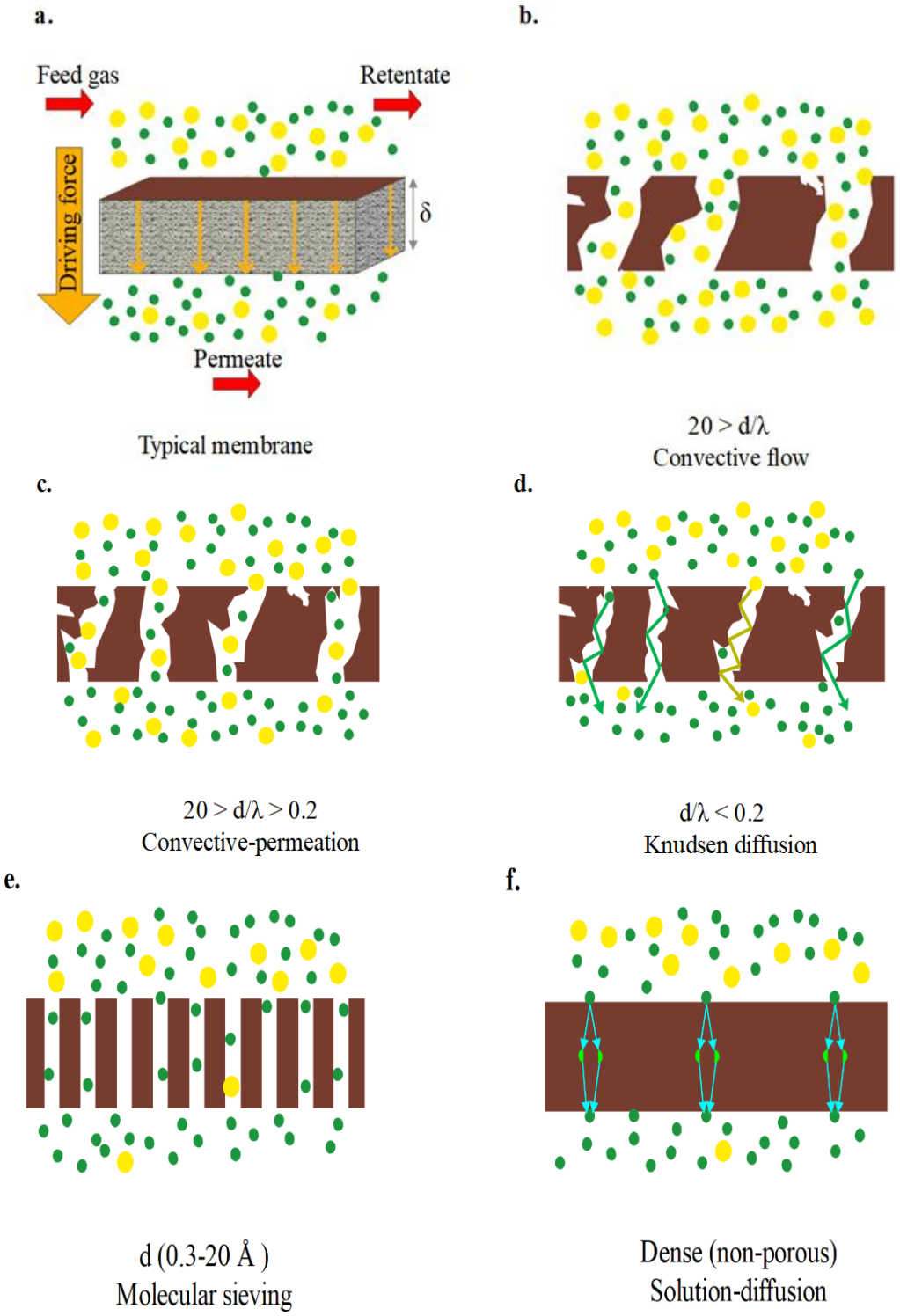


Figure 3. Separation mechanisms in membrane: (**a**) typical membrane, (**b**) convective flow, (**c**) convection–permeation, (**d**) Knudsen diffusion, (**e**) molecular sieving and (**f**) solution–diffusion [65]. Adapted with permission from Elsevier. Copyright 2021.

Characterization of Membranes

Membrane production procedure may include phase inversion, interfacial polymerization, and coating. The casting solution and cooling bath utilized in the phase inversion process have a substantial effect on the tortuosity, pore size distribution, pore network. morphology, microstructure, and mechanical properties. Fouling, conditioning, chemical exposure, disintegration, cleaning, the aging process can result in reversible or irreversible alterations to the physical and chemical properties of membranes; thus, membrane characterization is an essential part of membrane manufacturing and maintenance [74]. Characterization techniques such as XRD, SEM, TEM, TGA, DSC, BET, Zeta potential analysis, and FTIR may be employed. SEM images in Figure 4a,b show cross-section PES membrane and irregular porous surface of PVDF membrane, respectively [75,76]. TEM image of Figure 4c shows components of a hierarchical layer of a TiO_2 nanowire membrane [77].

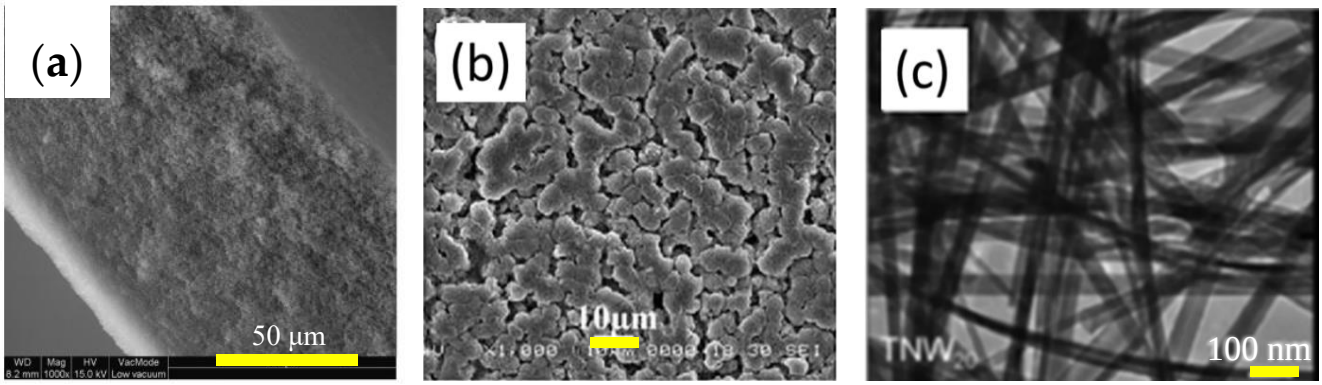


Figure 4. (**a**) Cross-section SEM images of PES membrane [76]. Adapted with permission from Elsevier. Copyright 2008, (**b**) top-view SEM images of PVDF membranes with irregular porous surface [75]. Adapted with permission from Elsevier. Copyright 2007, and (**c**) TEM images showing components of a hierarchical layer of a TiO_2 nanowire membrane [77]. Adapted with permission from water and research technology. Copyright 2015.

3. Configurations of PMRs

A typical PMR includes a light source, membrane, and photocatalyst [78]. The design and configuration of the PMR dictates process efficiency and controllability. PMRs are classified into two types based on the photocatalyst loading. As schematically illustrated in Figures 5 and 6, suspended photocatalytic membrane reactors (SPMR) are those in which the photocatalyst is suspended, whereas immobilized photocatalytic membrane reactors (IPMR) are those in which the photocatalyst is fixed on a carrier material such as quartz, stainless steel, glass, limestone, or zeolite [79]. When a photocatalyst is immobilized on a support, the active surface available to solution particles is drastically decreased, resulting in a loss of photoactivity [80]. The active surface increases significantly when the photocatalyst is suspended; however, after detoxification, the photocatalyst particles must be separated from the treated water. Table 2 shows the numerous applications of PMRs in wastewater treatment processes.

Benefits of PMRs over traditional photoreactors include: (1) the ability to regulate the residence inside the reactor; (2) continuous operation; (3) the containment of the contaminants and photocatalyst within the reaction environment; (4) enhancing process efficiency and stability; and (5) reduced reactor volume and operating costs [36,42,81].

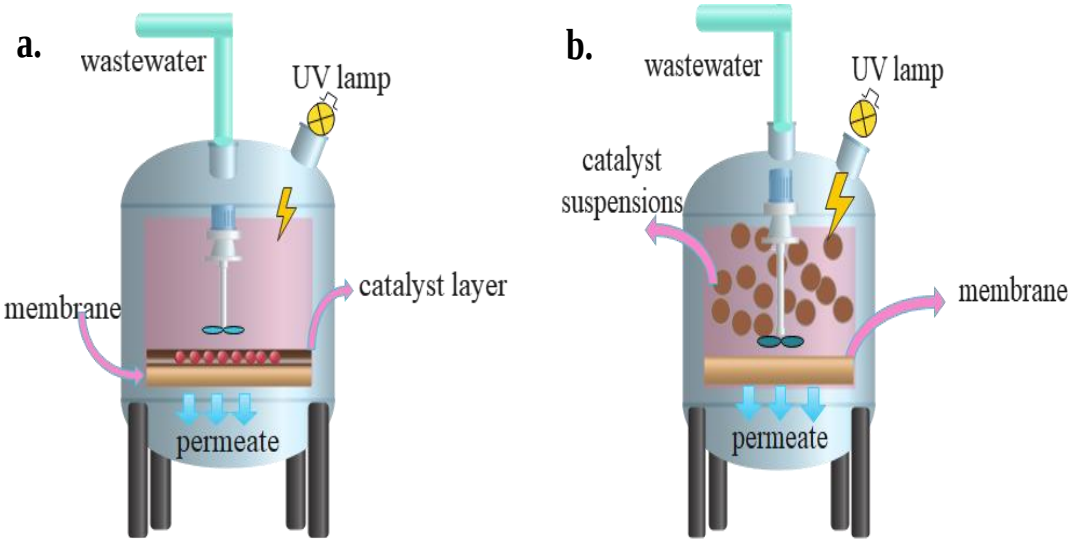


Figure 5. Two different configurations of PMRs (**a**) photocatalyst immobilized in/on the membrane, (**b**) photocatalyst in suspension media.

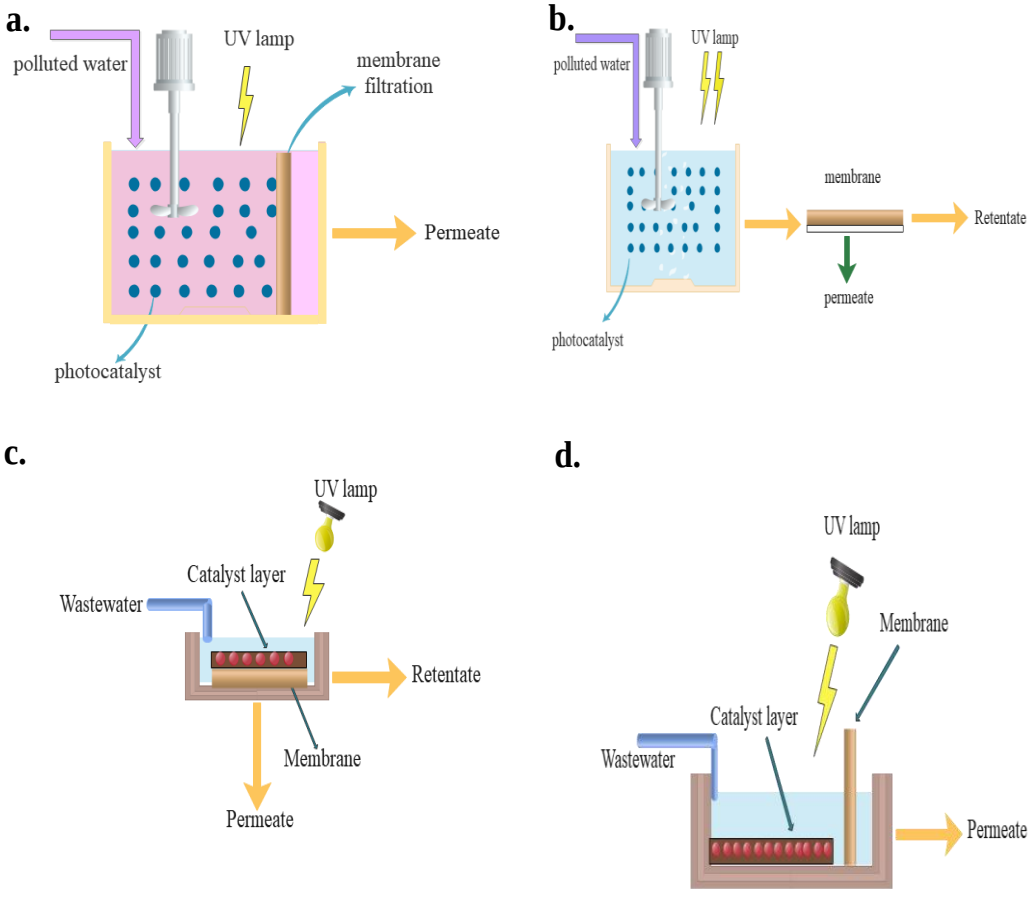


Figure 6. (**a**) Submerged membrane in a slurry reactor, (**b**) Slurry reactor followed by a membrane filtration unit, (**c**) Photocatalytic membrane, and (**d**) Submerged membrane in photocatalytic-coated reactor.

Table 2. Application of PMRS in wastewater treatment process.

Photocatalyst	Pollutant	Type of PMR	Photocatalyst Dosage (wt%)	Pollutant Concentration ($mg \cdot L^{-1}$)	Light Source	Time (min)	Degradation (%)	Ref.
P-doped g-C_3N_4 (PCN) and coated on an Al_2O_3 substrate	phenol and methyl blue		10	-	visible	-	92 and 90	[82]
MIL-88B(Fe) and coated onto an Al_2O_3 substrate	phenol		-	-	visible	-	-	[83]
immobilized N-doped TiO_2	diclofenac	SPMR	-	-	visible	-	-	[84]
MIL-53(Fe)/PVDF mixed-matrix membrane	tetracycline	IPMR	5	-	UV	-	93	[85]
UVA/TiO_2-MF	oxytetracycline	Suspended vs immobilized TiO_2-P25	-	5	visible	30	>90	[86]
polysulfone/H_2O_2-g-C_3N_4 mixed matrix membrane	humic acid	-	10	-	visible	-	93.5	[87]
NH_2-MIL125(Ti) MOF	methyl blue	immobilized and suspended	2	-	UV	-	60 and 97	[88]
TiO_2	ketoprofen	SPMR	-	10		-	61	[79]
TiO_2-WO_3/PANI	Cr (VI)	SPMR	5	-	Visible	60	98.5	[89]
TiO_2/UV-A	nitrate	SPMR	-	-	UV	-	65–90	[90]
TiO_2	ketoprofen	SPMR	-	10	-	-	75	[79]
Sb_2O_3/$CuBi_2O_4$	methyl blue	SPMR	10	10	Visible		94.6	[91]
ZnO/WO_3	phenol	SPMR	-	30		7	92.5	[92]

4. Photocatalytic Degradation of Pollutants

Many organic and inorganic substances, especially toxic or refractory substances are resistant to biological degradation. After the discovery of the photocatalytic splitting of water in 1972 by Fujishima and Honda [93], scientists and researchers turned their attention to semiconductor photocatalysts that could destroy resistant contaminants that were difficult or impossible to remove by other methods [94]. Photocatalytic degradation has emerged as one of the most sustainable, energy efficient, cost-effective and non-hazardous and environmentally friendly processes for contaminants removal from water which uses light as the energy source [95]. The catalyst's photonic activation mode, which replaces thermal activation, is the primary distinction between photocatalysis and traditional catalysis [96]. Photocatalysts do not contain heavy metal and do not require strong oxidants/reducing agents for activation. Photocatalysis degradation products are harmless [47].

4.1. Photocatalytic Degradation of Pharmaceutical Compounds

pH is one of the most vital factors that affects photodegradation efficiency. The efficiency of TiO_2 and ZnO nanoparticles in removing acetaminophen from the water was studies by Ahed et al. [97]. The outcomes of the study demonstrated that ZnO was more effective at eliminating acetaminophen. Ahed et al. proved that pH is an important factor in photodegradation. Their synthesized ZnO photodegraded 97% of acetaminophen at pH = 9 in 1 h of exposure. They demonstrated that at neutral pHs, photocatalytic degradation rates are higher than at acidic pHs. Sabouni et al. [98] investigated the elimination of progesterone, ibuprofen, and naproxen using ZnO photocatalyst. They studied the initial concentration of pollutants and the photocatalyst loading. They found that ZnO photocatalyst is quite efficient in eliminating all three pollutants. They reported progesterone, ibuprofen, and naproxen as having a degradation efficiency of 92.3%, 94.5%, and 98.7%, respectively. The degradation of paracetamol using TiO_2 and Fe_2O_3 photocatalysts was studied by Abdelwahab et al. SEM, TEM, XRD, FTIR, Raman spectroscopy, and VSM analyses were used to characterize the synoecized photocatalysts. Their results revealed that paracetamol degradation increased when TiO_2 loading in the TiO_2/Fe_2O_3 composite was increased [99]. The FTIR spectra of iron glycolate, Fe_2O_3, and 50% TiO_2/Fe_2O_3 reported by Abdelwahab et al. are displayed in Figure 7a. The peaks at 3432 cm^{-1} and 1618 cm^{-1} are

attributed to the O-H stretching and bending vibrations of adsorbed water or EG, respectively. Peaks between 2850–2950 cm^{-1} are indicative of C-H vibrations. Between 1120 and 1470 cm^{-1}, the CH_2 bending vibration peaks could be seen. C-O stretching vibrations were responsible for two sharp peaks at about 1050 and 1085 cm^{-1}. Peaks of the Fe-O stretching vibration were seen at the 467–660 cm^{-1}. All of the peaks related to the glycolate moiety have disappeared in the Fe_2O_3 FTIR spectrum, which was obtained after the iron glycolate was calcined at 350 °C [99].

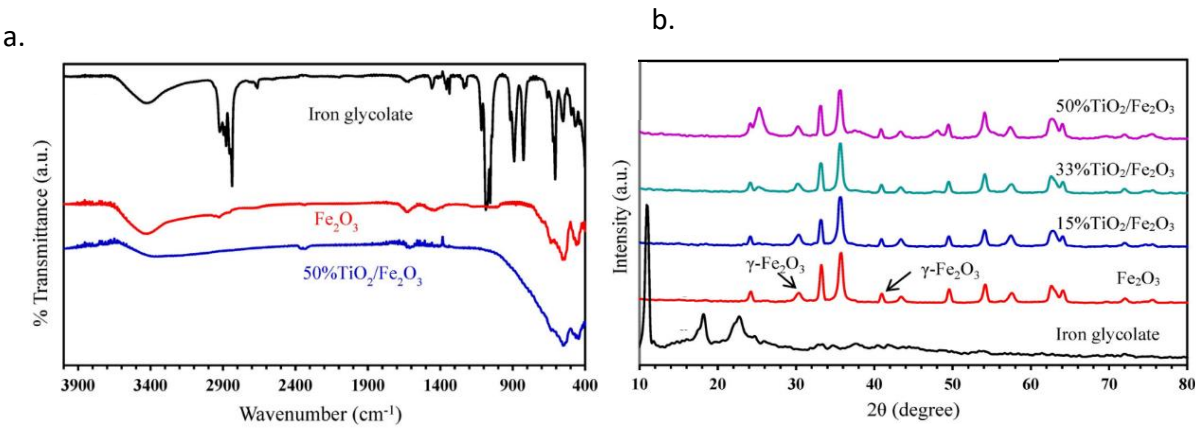


Figure 7. (**a**) FTIR spectra of iron glycolate, pure Fe_2O_3 microflowers and 50%TiO_2/Fe_2O_3 core-shell and (**b**) XRD patterns for iron glycolate, pure Fe_2O_3 microflowers and TiO_2/Fe_2O_3 core-shells [99]. Adapted with permission from Elsevier. Copyright 2017.

To examine the crystalline structure and phase purity of the prepared sample, the XRD patterns photocatalysts synthesized by Abdelwahab et al. are reported at Figure 7b. When the iron glycolate sheets are stacked, a prominent low-angle diffraction peak at 11° is observed. The diffraction pattern of the Fe_2O_3 product created by calcining the iron glycolate at 350 °C shows that the main diffraction peaks match with the α-Fe_2O_3 rhombohedral structural pattern. However, two peaks at 2θ of 30 and 43° that are either indicative of Fe_3O_4 or γ-Fe_2O_3 show that the acquired sample could be made up of α-Fe_2O_3 and other iron oxide crystal forms. the relative magnitude hematite (α-Fe_2O_3) and maghemite (γ-Fe_2O_3) and/or magnetite (Fe_3O_4) are 70% and 30%, respectively. Furthermore, the new peaks at 2θ of 25.2, 37.4, 48, and 54° of the TiO_2/Fe_2O_3 samples can be correlated to the (101), (004), (200), and (105) planes of anatase TiO_2, demonstrating that the TiO_2 crystallites were placed onto the magnetic core Fe_2O_3. The average crystallite size of TiO_2, calculated by Scherrer's equation is 12 nm for the anatase (101) peak [99].

Table 3 shows the photocatalytic degradation of different pharmaceuticals. Clearly, heterogeneous photocatalysts with a variety of nanostructures can effectively degrade pharmaceuticals in aqueous solutions.

Table 3. Review on Photocatalytic degradation of pharmaceutical compounds.

Pollutant	Pollutant Concentration ($mg \cdot L^{-1}$)	Photocatalyst	Light Source	Time (min)	Degradation (%)	Ref.
Carbamazepine (CBZ)	2.5	Z-scheme FeS_2/Fe_2O_3 /hexavalent chromium	simulated visible light	30	65	[100]
Penicillin G (PG)	5	TiO_2/P25	UV-A sunlight (365 nm)	150	72.72	[101]
Pentachlorophenol (PCP)	10	$FeNi_3/SiO_2/ZnO$	Irradiation of solar light	180	92.47	[102]
Ciprofloxacin (CIP)	10	Nano-ZnO	UV	30	96	[103]
Diclofenac (DCL)	1	ZnO	LP Hg (150 W)	30	68	[104]
Sulfamethoxazole	25	TiO_2	UV	150	61.28	[105]
Sulfamethoxazole	25	WO_3	UV	150	43.3	[105]

Table 3. *Cont.*

Pollutant	Pollutant Concentration (mg·L^{-1})	Photocatalyst	Light Source	Time (min)	Degradation (%)	Ref.
Dexamethasone (DXM)	5	ZrO_2/WO_3	halogen	80	100	[106]
Metronidazole (MNZ)	80	illuminated TiO_2	UV (125 W)	180	96.55	[107]
Levofloxacin	50	BiOCl(25)/BiOBr-$Bi_{24}O_{31}Br_{10}$(75) type-II nano heterojunction	Halogen (400 W)	180	80.2	[108]
Ofloxacin	50	BiOCl(25)/BiOBr-$Bi_{24}O_{31}Br_{10}$(75) type-II nano heterojunction	Halogen (400 W)	180	78.3	[108]
Amoxicillin metformin	10	TiO_2	125 W low-pressure mercury vapor lamp	150	90 98	[109]
Paracetamol	100	La-doped ZnO	fluorescent lamps (20 W)	180	99	[110]
Cefixime	20.5	α-Fe_2O_3@TiO_2	Visible	103	98	[13]
Cefixime	47	g C_3N_4/TiO_2	Visible	113	84	[111]

4.2. Photocatalytic Degradation of Dye Compounds

Dyes are routinely used in the textile, food, beverage, printing, and pharmaceutical industries. These compounds may be harmful and cancerous will barricade sunlight from reaching water bodies, impacting natural aquatic processes such as photosynthesis and other biodegradation operations [112,113]. Long-lasting and non-degradable colored pollutants must be removed before entering the environment since their entry leads to the aquatic ecosystem becoming toxic and dangerous to humans [114]. The photocatalytic process has been suggested as one of the more successful methods. In photocatalysis, the degradation is begun with OH radicals breaking the azo bond (-N=N-), which is one of the weakest chemical bonds in the dye molecules' chemical structure [115]. The process's intermediates will then undergo a radical chain reaction with the oxygen molecules, finally breaking down to produce water and carbon dioxide [115]. In recent years, numerous studies on the removal of contaminants from actual wastewater have been conducted. Table 4 illustrates the photocatalytic degradation of a variety of dyes.

Table 4. Review on Photocatalytic degradation of dye compounds.

Pollutant	Pollutant Concentration (mg/L)	Photocatalyst	Synthesis Method	Light Source	Time (min)	Degradation (%)	Ref.
Acid fuchsine (AF)	120	TiO_2/ACF	Sol–gel-adsorption	Hg lamp (500 W)	30	77	[116]
4-chlorophenol (4-CP)	15	ZTPG	High-temperature refluxing	UV	180	94.8	[117]
Methylene blue (MB)	20	ZTPG	High-temperature refluxing	UV	90	98.05	[117]
Basic Red 51 (BR51)	1	ZnO	-	sunlight irradiation	330	89.01	[118]
Methylene blue (MB)	9.56	ZnO	-	UV	30	93	[119]
Methyl Orange (MO)	5	TiO_2/MgO/Chitosan	Hydrogel	UV (125 W)	90	82.4	[120]
Alizarin Red S (ARS)	5	TiO_2/MgO/Chitosan	Hydrogel	UV (125 W)	90	41.8	[120]
Methyl Orange (MO)	15	Ni@FP + $NaBH_4$ (10 mg)	-	UV	5	93.40	[121]
Tartrazine	50	$CuCr_2O_4$	self-combustion	Hg lamp (125 W)	120	99.6	[122]
Acid Brown 98	10	CS-ZnS-NPs	co-precipitation	UV (254 nm)	165	92.6	[123]
Acid Black 234	10	CS-ZnS-NPs	co-precipitation	UV (254 nm)	100	96.7	[123]
Methylene blue (MB)	3.2	$MnTiO_3/TiO_2$	sol-gel	sunlight	240	75	[124]
Tartrazine	10	TiO_2–Chitosan	-	Sunlight	180	99.37	[125]
1,2-Dichloroethane	250	PAni-TiO_2	deposition oxidative polymerization	visible	240	88.84	[126]

4.3. Photocatalytic Degradation of Hydrocarbons

Industrial use of hydrocarbons inevitably contaminates natural waters through improper disposal or leaching from landfills, spills, or leaks in underground pipes. Hydrocarbon contaminants endanger human health if they enter drinking water. The presence of these contaminants in water hinders light penetration into the water and affects the diffusion/solubility of gases required for aquatic plant respiration which ultimately leads to plant death; therefore, it may affect the food supply chain.

Schnabel et al. [127] used semiconductor titanium dioxide to remove hydrocarbons. This study demonstrated that a variety of photocatalyst designs, when exposed to ultraviolet (UV) light, can remove the non-polar material in diesel fuel. They reported that the floating foam glass catalyst with TiO_2 coating reduces the concentration from an initial concentration of 668 mg/L to 329 mg/L in 16 h. The contaminant concentration is reduced by 401 mg/L and 55 mg/L when glass fiber and steel grit was used, respectively [127].

Nirmala Rani et al. [128] studied the elimination of three polycyclic aromatic hydrocarbons (PAHs) in mixed or separate states using titanium oxide photocatalysts and MS membranes under UV irradiation in a PMR. They reported the degradation efficiency of 100, 94.1, and 97% in an aqueous mixture containing 1000 µg /L phenanthrene (PHE), 5000 µg/L naphthalene (NAP), and 1000 g/L acenaphthene (ANA), respectively, after 180 min UV irradiation at photocatalyst loading of 0.5 g/L. When the compounds were used as a sole compound, the elimination percentages of PHE, NAP, and ANA were 99.3, 92.8, and 95.3, respectively, under similar operating conditions [128,129]. The photocatalytic degradation of several hydrocarbons is reported in Table 5.

Table 5. Review on Photocatalytic degradation of hydrocarbons.

Pollutant	Pollutant Concentration (mg/L)	Photocatalyst	Synthesis Method	Light Source	Time (min)	Degradation (%)	Ref.
Benzene Toluene Phenol Naphthalene	65	TiO_2	-	UV (400 W)	90	92 98.8 91.5 93	[130]
Paraffin	500	TiO_2/SiO_2 thin film	sol-gel	UV	180	85	[131]
BTEX TPHs	60.8	TiO_2	-	solar light	240	>70	[132]
Naphthalene	50	ZnO/Ag/GO nanocomposit	-	Xe lamp (250 W)	20	80	[133]
BTEX	600	γ-Fe_2O_3 nanoparticle	-	UV light (100 W)	90	97	[134]
Naphthalene	40	Calcinated Fe-doped ZnO/PVA nanofibers	-	UV light (16 W)	360	96	[135]
Chrysene	2	Fe_2O_3@ZnHCF nanocubes	-	sunlight	1440	92	[136]
Benzene, toluene and xylenes (BTX) and gasoline-contaminated waters	20	TiO_2-Fenton system	-	medium-pressure mercury vapor lamp (125 W)	90	75	[137]
Formaldehyde	700	MIL-100(Fe)	solvothermal	Visible	119	93	[138]

4.4. Photocatalytic Degradation of other Pollutants

Photocatalyst have been used to degrade pollutants listed in Table 6. Pitchaimani Veera Kumar et al. [139] employed zinc oxide nano stars (ZnONSt) coupled with Ag and Pd to photocatalytically degrade herbicides and pesticides. Ag at ZnONSt and Pd at ZnONSt photocatalysts accelerated the degradation of existing pollutants as they facilitate the interfacial charge transfer process [139]. In order to remove the herbicide ametrine, Rodrigo Pereira Cavalcante et al. [140] utilized a titanium dioxide photocatalyst. They were able to completely remove the ametrine after 60 min irradiation of simulated sunlight (using a 1000 W Xenon lamp), and then they used 0.4 g/L of photocatalyst to detoxify the solution. Samsudin et al. [141] utilized $BiVO_4$/g-C_3N_4 integrated with Pt to purify poultry during sun light exposure. The as-synthesized photocatalyst demonstrated 93.5% COD

removal from the starting concentration of 2152 mg/L in 3 h. The photocatalyst showed strong recyclability and photostabiliy.

Table 6. Review on Photocatalytic degradation of other pollutants.

Pollutant	Pollutant Concentration (mg/L)	Photocatalyst	Synthesis Method	Light Source	Time (min)	Degradation (%)	Ref.
Bisphenol-A (BPA)	50	$ZnFe_2O_4$/leaf extract of Azarachita indica	-	sunlight	720	92	[142]
Bisphenol-A (BPA)	50	$CoFe_2O_4$/leaf extract of Azarachita indica	-	sunlight	720	89	[142]
Bisphenol-A (BPA)	50	Fe_2O_3/leaf extract of Azarachita indica	-	sunlight	720	70	[142]
Bisphenol-A (BPA)	50	ZnO/leaf extract of Azarachita indica	-	sunlight	720	68	[142]
Bisphenol-A (BPA)	50	Co_3O_4/leaf extract of Azarachita indica	-	sunlight	720	54	[142]
Para-aminobenzoic acid	20	TiO_2 P25	-	UV (9 W)	120	>80	[143]
toluidine blue o, safranin o, falcon carboxylic acid, Hexavalent chromium Cr	5	ZnO	-	UV light (250 W)	190, 310, 260, 300	94, 87, 92, 68	[144]
Hexavalent chromium Cr (VI) bisphenol A (BPA)	10	magnetic 3D-TiO_2@HPGA	solvothermal process	low pressure mercury vapor lamps (8 W)	140 240	100 90	[145]
Clofibric acid (CA)	2	g-C_3N_4	-	Xe-lamp (350 W)	<50	46.8	[146]
Clofibric acid (CA)	2	P25	-	Xe-lamp (350 W)	<50	56.8	[146]
Clofibric acid (CA)	2	g-C_3N_4/P25 (8 wt%)	-	Xe-lamp (350 W)	<50	85.4	[146]
Atrazine	100	Cu-ZnO/g-C_3N_4 Z-direct scheme	-	UV	120	90	[147]
Herbicide glyphosate	100	BiOBr/Fe_3O_4 nanocomposites	Chemical co-precipitation method	Xe lamp (500 W)	60	97	[148]
Diuron herbicide	25	g-C_3N_4/N-doped CeO_2 composite	-	Xe lamp (1500 W)	120	46	[149]
Gramoxone herbicide	10	TiO_2 hollow fibers	-	UV lamp (6 W)	480	<50	[150]
Chlorpyrifos	2	$CeO_2/TiO_2/SiO_2$	sonophotocatalytic	Visible	150	90.8	[151]

5. PMRs

5.1. Operating Factors and Limits of PMRs

5.1.1. Operating Mode

Both dead-end and cross-flow PMRs can be used in photocatalytic systems. In the dead-end configuration, the whole stream is filtered by passing through a membrane (permeate). As a consequence, the concentration of the nontransferable components rises, resulting in creation of a filter cake on a membrane's surface, as well as a reduction in membrane permeability and photocatalytic efficiency. In the absence of turbulency, e.g., stirring, there will be insufficient contact between the contaminants, photocatalyst, and the light source [152]. Wang et al. [153] investigated a novel photocatalytic membrane created via pressure-driven filtration load with a ZnO/N-g-C_3N_4 composite via glutaraldehyde as a crosslinker. SEM, XPS, and FTIR were employed to verify the photocatalyst loading on membrane surface. They found that in both immersion and filtration models, the photocatalytic capabilities of the ZnO/N-g-C_3N_4 composite membrane were effective for the decomposition of tetracycline, ofloxacin, and ciprofloxacin under visible light (>420 nm). For tetracycline at 5 mg/L and 10 mg/L concentrations a ZnO/N-g-C_3N_4 loading of 1.12 g/cm^2 resulted in 100% and 80% degradation, respectively. They concluded that a pro-

longed reaction time on the membrane surface, low trans-membrane pressure (0.005 MPa), and narrow membrane size were advantageous for the elimination of antibiotics in the filtration processes.

5.1.2. Photocatalyst Type and Characteristics

Key parameters that significantly affect photocatalytic efficiency include the type of photocatalyst, the photocatalyst's physicochemical properties (band gap energy, particle size distribution, crystallographic structure, and chemical makeup), and the photocatalyst's concentration in the reacting environment. As mentioned previously, photons by energy equal to or greater than the band gap energy can be absorbed in photocatalytic activities, resulting in the creation of electron-hole pairs. However, photocatalysts that require visible light to function are more intriguing, and it has become a challenge for PMR systems to use a light source that is both environmentally friendly and economically viable [154]. For example, TiO_2-supported photocatalyst is the most frequently employed in PMR in suspended form due to its great photochemical stability in aquatic solutions, robust catalytic activity, reasonably long lifespan of electron-hole pairs, low cost, and low toxicity. This material is inactive when exposed to visible light. As a result, TiO_2 can only absorb around 5% of the solar radiation that is in the UV spectrum [155]. Ahmad et al. [156]. stated that a developed composite ceramic membrane may benefit from a synergy of dead-end filtration and cross-flow filtration while being subjected to intermittent UV irradiation in order to efficiently prevent membrane fouling. To remove organic dye impurities in a photocatalytic membrane reactor, a partly coated TiO_2 (pc-TiO_2) layer was made with the assistance of cheap polyvinyl chloride (PVC) to make gaps in a porous Al_2O_3 membrane substrate. Their study revealed that the pc-TiO_2/Al_2O_3 composite membrane has superior water flux and anti-fouling capabilities compared to the uniformly coated TiO_2/Al_2O_3 (UC-TiO_2/Al_2O_3) membrane. The photocatalytic activity of UC-and pc-TiO_2/Al_2O_3 composite membranes was significantly enhanced during cross-flow membrane filtration in comparison to that of the Al_2O_3 bare membrane substrate.

5.1.3. Light Source

When light is shone on photocatalysts, photons with energy higher than or equal to the band gap are absorbed, valence band electrons are shifted to the conduction band. The oxidation and reduction reactions that occur are due to the production of electron-hole pairs [4]. Consequently, the kind and intensity of light have a significant impact on the performance of photocatalysis [157].

The sol-gel procedure and the dip-coating may be used to create a nanostructured TiO_2 film from titanium tetraisopropoxide. Sol-gel nanostructured TiO_2 (anatase phase) film was investigated for its photocatalytic degradation of azithromycin to determine the most efficient degradation pathway for application in wastewater treatment. At the pH of 10 and UV-C irradiation maximum degradation was achieved. The LED irradiation source with emission wavelength of 365 nm was not as efficient as the UV-C lamp. The LED bulb, however, may be a "real-world" option due to its low price, high energy efficiency, and low environmental impact [158]. Shang et al. [159]. investigated the antibacterial activities of TiO_2 photocatalysts under various light sources, exclusively under visible light. They discovered that by doping metal ions and nonmetal ions on TiO_2 and compounding with polymers, they could increase the photocatalytic activity to the visible light region, improve the surface characteristics, and enhance the contact area with bacteria. Reactive oxygen species (ROS) and hydroxyl free radicals damage the cell membrane, DNA, and enzymes.

5.2. Degradation of Pharmaceutical Compounds via PMR

Pharmaceutical compounds are structurally complex and environmentally stable. They typically contain abundant aromatic rings. Thus, conventional wastewater treatment methods cannot effectively remove them. Hence, the use of PMRs has become a popular solution for removal of pharmaceutical compounds from water. Fang et al. [153] synthe-

sized a ZnO/N-g-C_3N_4 composite and immobilized it on a commercial polymer membrane via GA as the crosslinker to breakdown antibiotics under visible light in a PMR setup. Additionally, the ZnO/N-g-C_3N_4 composite photocatalytic membrane properties were evaluated using the immersion model and the filtration model. The amount of ZnO/N-g-C_3N_4 loading and GA concentration were significant for the photocatalytic abilities of composite membranes, according to an immersion model. The outcome demonstrated that the filtering model results in a greater antibiotic decomposition at longer photocatalytic reaction time, that could be attained by narrow membrane pore sizes, low TMP, and reduced flow. Using a similar photocatalytic membrane fabrication procedure using pristine membrane with MWCO of 50 kDa, improved TC degradation (71.7%) was obtained by the immersion approach which is attributed to the decreased flux and increased retention time. The Photocatalytic membrane degradation of pharmaceutical compounds is shown in Table 7.

Table 7. Review on Photocatalytic Membrane degradation of pharmaceutical compounds.

Pollutant	Pollutant Concentration (mg/L)	Photocatalyst/Synthesis Method	Membrane/Pore Size (µm)	Light Source	Time (min)	Degradation (%)	Ref.
Chloramphenicol	50	TiO_2 doped hydroxyapatite/hydrothermal	polysulfone (PSF)/0.003	UV Light	120	61.59	[160]
Pharmaceutical industry wastewater	TDS 4740 COD 17360	Cerium fluoride (CeF)/Phase inversion by immersion precipitation technique	polysulfone (PSF)	24 W UV lamp		97	[161]
Triclosan	10	bismuth vanadate/polyethyleneimine blended in polyethersulphone		300 W Xenon Lamp		86	[162]
Sulfamethoxazole	10	mesoporous graphitic carbon nitride/TiO_2		300 W ozone free xenon lamp		49	[163]
Sulfadiazine	12	Goethite (α-FeOOH)/precipitation	0.14	UVL214W lamp		70 (no H_2O_2) and 99 (with H_2O_2)	[164]
Diclofenac	10	N, S-CQDs/TiO_2	polysulfone (PSF)	light (40 W), visible light (12 W)	150	62.3	[165]
Oxytetracycline	20	TiO_2	UF membrane	UVC lamp (16 W)		52 DOC removal	[166]
Diphenhydramine	-	graphene oxide-TiO_2	Mixed cellulose ester (MCE)	UV/Vis and visible light irradiation		73	[167]
Chlorhexidine Digluconate	-	TiO_2	PES and PVC-PAN	1500 W solar simulator		40	[168]
Diclofenac	2	TiO_2	PVDF/0.04	4 × 24 W black Light		99.5	[169]
Diclofenac and ibuprofen	Diclofenac sodium salt 25, ibuprofen sodium salt 100	TiO_2	PES and PVDF/0.22	7.6 mW/cm^2 UVA lamp	120	For PES 68, For PVDF 55	[170]
Diclofenac (DCF), ibuprofen (IBU) and naproxen (NAP)	100 µg dm^{-3}	TiO_2	Polypropylene (PP)/0.2	16 W UVC germicidal lamp		DCF100, IBU 73, NAP 90	[171]
furosemide, ranitidine, ofloxacine, phenazone, naproxen, carbamazepine	10	TiO_2	different NF membranes (PES, PSF, PAN)	125 W medium pressure Hg lamp	120	furosemide 80, ranitidine 50, Naproxen 90	[172]
tetracycline	5	Au/Ag/TiO_2	CA/0.213	Xe lamp		90	[173]
Diclofenac	0.05	TiO_2	PVDF/0.03	52 W UV-C power		100	[174]
Tetracycline	10	Au-TiO_2	PDA-PVDF/0.22	Xenon lamp	120	90	[175]
Diclofenac	50 for batch 20 for continuous	N-doped TiO_2	MF membrane 0.1, RO membrane 0.0001–0.001	5 × visible 250 W lamps	150–180	97.66	[84]
Ciprofloxacin	10	sulfonated graphene oxide/ZnO	PES/0.011	150 W UV	240	95.1	[176]

Table 7. *Cont.*

Pollutant	Pollutant Concentration (mg/L)	Photocatalyst/Synthesis Method	Membrane/Pore Size (μm)	Light Source	Time (min)	Degradation (%)	Ref.
Pharmaceutical industry wastewater	TDS 4740 COD 17360	ZrO_2–SnO_2/sol-gel	PS	24 W UV lamp		90	[177]
Tetracycline	10	$ZnIn_2S_4$	PVDF/0.3	150 W halogen tungsten lamp		50	[178]
Carbamazepine	1	α-Al_2O_3 coated with N-doped TiO_2/Sol-gel	0.2–0.8	300 W ozone-free xenon arc lamp		90	[179]

5.3. Degradation of Dye Compounds via PMR

Synthetic paint is one of the most abundant pollutants in sewage and effluent of industrial plants. The most commonly investigated dyes are rhodamine B, methylene blue, and methyl orange. Conventional wastewater treatment methods are inefficient in removing dyes. Photocatalytic technology is one of the most successful approaches suggested for dye removal.

Dzinun et al. [180] create a TiO_2-PVDF photocatalytic membrane by addition of different loading of TiO_2 nanoparticles on a PVDF membrane for methylene blue removal. They characterized the resulting photocatalytic membranes with FE-SEM, EDS, and AFM. The results of their custom-designed PMR demonstrated that adding TiO_2 nanoparticles to the PVDF membrane speeds up methylene blue removal from waste water. Kolesnyk et al. [181] studied the impact of g-C_3N_4 loading on a commercial PVDF membrane on rhodamine-B removal. The highest removal rate occurred in the alkaline medium. In this study, the membrane lost approximately 15% of its pores after five cycles (a total of 50 h). Yu et al. [163] synthesized a PSF membrane coated with g-C_3N_4 and TiO_2 nanocomposites to investigate the removal of sulfamethoxazole. They reported that sulfamethoxazole was converted into seven other non-toxic substances using their custom-designed PMR with sun light irradiation [163]. Horowitz et al. [179] investigated the efficiency of Al_2O_3 coated membranes with pore sizes of 200 and 800 nm for carbamazepine removal at different operating conditions. It was observed that the PMR efficiency under UV irradiation is much higher than that under visible waves. They also reported that the contaminant removal rate increases with temperature. Ma et al. [182] investigated humic acid removal from wastewater using TiO_2/Al_2O_3 photocatalyst and membrane microfiltration processes. They found that light intensity significantly affects humic acid removal. A summary of dye degradation via PMRs is reported in Table 8.

5.4. Degradation of Hydrocarbons via PMR

Rani et al. used a membrane photocatalytic reactor containing suspended TiO_2 photocatalytic particles for naphthalene removal. They studied the impact of different operating parameters such as the initial concentration of naphthalene (5–25 mg/L), photocatalyst loading (0.1–0.9 g/L), and pH (3–9) on naphthalene removal rate. The maximum naphthalene removal by separate photocatalysis and membrane was 76.8% and 49.1%, respectively, while a naphthalene removal of 90.2%. could be achieved by PMR [183]. Batch PMRs functioning in the dead-end mode was designed by Moslehyani et al. [184] which could to eliminate 99% of the hydrocarbons from sludge after 2 h. Ag-TiO_2-coated alumina membrane in a dead-end configuration to degrade rhodamine rate of 1.007 mg/m^2h^1 [185]. Despite the promising outcomes, the researchers emphasized that the dead-end process leads to the buildup of separated substrates on the membrane surface and ultimately forms a cake layer, which decreases photocatalytic efficiency. A summary of hydrocarbon degradation via PMRs is reported in Table 9.

5.5. Degradation of Other Pollutants via PMR

Pollutants such as toxins, detergents, and heavy metals that do not fall into the above categories are also treated by PMRs which can be seen in Table 10. For example, it can be seen from Table 10, 99.9% of toxic hexavalent chromium (Cr (VI)) at an initial concentration of 10 mg/L could be removed by PMR containing Chitosan-sodium alginate/Fe-doped WO3 photocatalyst and PES membrane after 240 min using a 300 W Xe light source [186].

Table 8. Review on Photocatalytic Membrane degradation of dye compounds.

Pollutant	Pollutant Concentration (mg/L)	Photocatalyst/Synthesis Method	Membrane/Pore Size (μm)	Light Source	Time (min)	Degradation (%)	Ref.
Phenol	50	TiO_2-GO/modified Hummer's	PVDF, PAA/0.45	100W UV-C lamp		60	[187]
RhodamineB	10	CNTs/MCU-C_3N_4/GO	PVDF	300 W Xe lamp,		98.31	[188]
RhodamineB	-	TiO_2	PVDF/0.08–0.2	3 UV-C lamps		95	[189]
Eosin yellow	100	N,Pd co-doped TiO_2/	Polysulfone	500 W Xenon lamp	180	92	[190]
Phenol	5	g-C_3N_4/CNTs	Al_2O_3/0.297	300 W Xe lamp	60	94	[191]
Methylene blue	1	TiO_2	Al_2O_3/0.02–0.2	UV-LED		80	[192]
Methylene blue	-	$ZnWO_4$/NiAl-LDH/Hydrothermal	PVDF/0.45 for pure PVDF		120	93.97	[193]
Methylene blue	500	Co/PC/g-C_3N_4		Xe Lamp 300 W	360	99	[194]
Methylene blue	1	NbCxOy/NbOx/g-C_3N_4	-	-	480	100	[195]
RhodamineB	10	TMPyP/SPSf/non-solvent-induced phase separation	PES	300 W Xe Lamp	180	93.4	[196]
Methylene blue	10	RGO/PDA/TiO_2/Hummer method	CA/0.3–0.52		150	80	[197]
Phenol	10	O-g-C_3N_4	PES/0.125–0.188	30W UV lamp,	120	35.78	[198]
RB5	30	Fe^{3+} doped ZnO	-	artificial sunlight (D65, 72W)	180	98.34	[199]
Methylene blue, RhodamineB, and methyl Orange	20	TiO_2/ hydrothermal	PPS/0.185	300 W Xenon lamp	90	RhodamineB 99.56, methylene blue 98.05, methyl Orange 93.18	[200]
Methyl orange	10	meso-TiO_2/	PVDF	25 W UV lamps	720	Higher than 90	[201]
Methylene blue	30	PDA/RGO/Ag_3PO_4/	PVDF	200 W incandescent lamp		99.1	[202]
Methyl orange	7.8	TiO_2 nanoparticles/Dip-Coating	Al_2O_3/0.125	300 W high-pressure mercury UV tube		61.2	[203]
RhodamineB	8	MWCNTs/Ag_3PO_4/combining electrospinning with in situ Ag_3PO_4 forming reaction	PAN	300 W Xe arc lamp	120	96.9	[204]
Methylene blue 4-CP	15	reduced graphene oxide (RGO)/poly(dopamine) (PDA)/$Bi_12O_17Cl_2$/	CA/0.22	500 W long-arc Xe lamp,	160	methylene blue 98, 4-CP 96	[205]
Methylene blue	10	TiO_2 nanoparticles/Electrospraying TiO_2 particles	Polyamide-6 nanofiber	300 W Osram Ultra-Vitalux lamp	360	99	[206]
Methylene blue	-	TiO_2/Magnetron sputtering	PES/0.45		160	70	[207]
Congo red	-	Fe-doped ZnO/rGO/Sol-gel	NF	solar radiation		87	[208]
Methylene blue	3.2	Graphene oxide	PVDF/0.1–0.7	150 W xenon lamp		83.3	[209]
Rhodamine 6G, Rhodamine B	5 to 50	Graphene oxide/direct heating of melamine	PVDF	LED lamp		Rhodamine B 96, Rhodamine 6G 94	[181]

Table 8. *Cont.*

Pollutant	Pollutant Concentration (mg/L)	Photocatalyst/Synthesis Method	Membrane/Pore Size (μm)	Light Source	Time (min)	Degradation (%)	Ref.
Methylene blue	1	PdTFPP	PVDF/0.2	4.6 W Green and white light emitting diode		83	[210]
Rhodamine B	10	g-C_3N_4/RGO/ photoreduction	CA/~0.430	Xe lamp	90	90	[211]
Methylene blue	50	nitrogen-doped graphene/TiO_2/ nonsolvent-induced phase-separation	PSF	125W UV lamp, 100 W fluorescent bulb	120	94.6	[212]
Remazol black B	50	g-PAA/ZnO	PVDF/0.45	15 W UV lamp	300	86	[213]
Rhodamine B	5	Bi_2O_3/ZnS/	CA/0.11–0.14	200 W xenon light	120	~85	[214]
Acid orange 7	50	$SrTiO_3$/TiO_2/ hydrothermal	CA/0.2	UV lamp		100	[215]
Methyl blue, phenol	methyl blue 5 phenol 3.3	Phosphorus-doped g-C_3N_4/ thermal condensation	Al2O3/0.18–0.2	300 W Xe lamp		Phenol 92, methyl blue 90	[84]

Table 9. Review on Photocatalytic Membrane degradation of hydrocarbons.

Pollutant	Pollutant Concentration (mg/L)	Photocatalyst/Synthesis Method	Membrane/Pore Size (μm)	Light Source	Time (min)	Degradation (%)	Ref.
Acenaphthene	1–3	TiO_2	PES	16 W Hg UV-C lamp		Batch process 95.1, Continuous process 80	[216]
Crude oil	100	TiO_2, $BiVO_4$, WO_3/hydrothermal	PVDF/0.1	14.4W LED strip		89	[217]
Roxarsone		$BiOCl_{0.875}Br_{0.125}$	PVDF			100	[218]
propranolol	2	TiO_2/rGO-TiF	0.160–0.175	UV lamp	60	35	[219]
Bisphenol	10	Ag-doped TiO_2/ Liquid impregnation—phase inversion	PESf	100 W Xe lamp	270	88	[220]
Naphthalene	5–25	TiO_2	PES	16 W Hg UV-C lamp	180	batch process 92.8, continuous process 93.1	[183]

Table 10. Review on Photocatalytic Membrane degradation of other Pollutants.

Pollutant	Pollutant Concentration (mg/L)	Photocatalyst/Synthesis Method	Membrane/Pore Size (μm)	Setup Configuration	Light Source	Time (min)	Degradation (%)	Ref.
BSA	-	$SrTiO_3$–Cr	PVDF	0.2–1 μm	UVA light		Higher than 98	[221]
Oil in water emulsions	-	GO/MCU-C_3N_4	PVDF	0.22		30	Higher than 96	[222]
Humic acid	20		Alumina-supported titania/0.657–0.425		mercury lamp with light emission of 1255 μW/cm^2	180 nin	92	[223]
Oily wastewater	500 and 1000	TiO_2	Al_2O_3/Ceramic membrane	-	UV lamp		90	[224]
Nitrate	10	$LiNbO_3$/phase inversion	PES	-	UV light	180	81.82	[225]
Oily wastewater	250–10,000	TiO_2-P25	PVDF	-	8W UV-A lamp	240	80 TOC degradation	[226]
BSA	1000	GO/TiO_2/PVP/ solution casting and phase inversion	PVDF	-	UVA irradiation	120	92.5	[227]

Table 10. *Cont.*

Pollutant	Pollutant Concentration (mg/L)	Photocatalyst/Synthesis Method	Membrane/Pore Size (μm)	Setup Configuration	Light Source	Time (min)	Degradation (%)	Ref.
Bentazone	10		N–TiO_2/PMAA/PVDF/ PAN/Loeb-Souriraja	-	UV-light and solar irradiation	180	90.1	[228]
Hexavalent chromium (0Cr (VI))	10	Chitosan-sodium alginate/ Fe-doped WO_3	PES	-	300 W Xe lamp	240	99.9	[186]

6. Membrane Fouling in PMRs

Different components of feed, such as organic substances, photocatalysts, colloids, salts, and cells, can have varying effects on system performance [229]. The fouling of PMR membranes is caused by the deposition of feed components on the membrane. Photocatalytic oxidation partially eliminates foulants [230]. Foulant adhesion, pore blocking, the cake layer formation, and temporal and spatial changes of foulant structure during long-term filtration are among factors that promote fouling [230,231]. Photocatalyst nano particles may form microaggregate and deposit on the membrane during filtration. Organic pollutants accumulation in the vicinity of membrane may result in formation of a very thin layer leading to substantial pore clogging and flow rate reduction. Adsorption of organic contaminants on TiO_2 particles and its composites such as Degussa P25 TiO_2, Ca alginate polymer/TiO_2 fibers, nano-structured TiO_2/silica gel photocatalyst, and titanium tetraisopropoxide in the absence of effective UV absorption may result in formation of a dense cake layer on the membrane surface and further flow rate reduction [232].

Designing non-fouling membranes is highly sought. Zheng et al. [233] combined the cellulose nanocrystals (CNCs) onto Cu-MOF-74 by physically stirring, and then coated the composites on the membrane to enhance the antifouling efficiency of PVDF membranes. CNC/Cu-MOF-74 composite coating on PVDF membrane increased its hydrophilicity, which in turn considerably improved the membrane's permeability and productivity. They also reported enhanced electrostatic repulsion based on the contact angle test and Zeta-potential measurement. Due to Cu-predominate MOF-74's antibacterial activity, the CNC/Cu-MOF-74 modified membrane also demonstrated increased antibacterial performance. effective antibacterial performance of composite membrane was attributed to Cu^{2+} release and •OH production.

6.1. Reactor Design

Modulating photocatalytic reactions, exchanging catalysts, and degrading pollutants are all easier with slurry PMRs. Although catalyst separation is not required for IPMRs, the catalyst loading cannot be tailored to the feed's specific composition; higher catalyst loading, larger membrane surface area, and higher-pressure drop are required which increases the reactor volume, energy consumption of pumps, and process cost. Exchanging the catalyst is also a challenging process especially in IPMRs [234,235].

6.2. Photocatalyst Loading

Membrane foulants can be reduced and photocatalytic degradation may be accelerated by increasing catalyst loading due to increase reaction surface area. [234]; however, photocatalyst loading has an optimum value for any specific process after which increased opacity of the reaction mixture hinders light absorption by photocatalyst [13,236]. Elevated photocatalyst loading results in reduced foulant degradation which enhances fouling rate on the membrane [237,238].

7. Conclusions and Future Perspectives

This review described various hybrid photocatalysis and membrane process designs for removing organic contaminants from water. The main advantage of PMRs is reten-

tion and reuse of photocatalyst. The advantages and disadvantages IPMRs and SPMRs, as well as important design/operation parameters were discussed. The performances of a photocatalytic reaction can be improved by utilizing a suspended photocatalyst as opposed to an immobilized one, owing to larger active surface and subsequently improved photocatalyst–substrate interaction. SPMR empowered by air bubbles and effluent flushing appears to be more suitable for treating water and wastewater. Visible light may be utilized as an irradiation source and efficient solar-driven photocatalytic conversion has emerged in recent years. The appropriate selection of the membrane is crucial, as it must have great permeability to the desired product and retain contaminants and photocatalyst to facilitate the rapid removal of the product from the reaction environment. When it comes to treating wastewater, TiO_2-based PMRs excel because of their excellent separation efficiency and low maintenance requirements. When designing visible-light-operated photocatalysts, it is important to examine the option of employing the sun as a clean, low-cost light source to make the process more environmentally friendly. Advantages of using PMRs for the partial oxidation and reduction of organic matter include (a) extending the lifetime of polymeric membranes with the help of visible light as a source of radiation, and (b) enhancing photocatalyst recovery through the use of novel materials in the synthesis of photocatalyst composites and semiconductor coatings on optical fibers. PMRs utilization has become a mode viable wastewater treatment option upon developments in photovoltaic technology (solar energy conversion) and the use of LED lamps (UV and/or visible).

Author Contributions: M.B. and S.M.M. developed the idea and structure of the review article. S.A.H. and J.R. wrote the manuscript and collected the materials from databases. S.M.M. and C.W.L. and S.S., revised and improved the manuscript. M.B. and S.S. and C.W.L. supervised the manuscript. All authors have read and agreed to the published version of the manuscript.

Funding: This research work was financially supported by Fundamental Research Grant Scheme FRGS/1/2020/TK0/UM/02/8 (No. FP023-2020), and Global Collaborative Programme—SATU Joint Research Scheme (No. ST004-2021).

Institutional Review Board Statement: Not applicable.

Informed Consent Statement: Not applicable.

Data Availability Statement: All data generated or analyzed during this study are included in this published article.

Conflicts of Interest: The authors declare no conflict of interest.

Abbreviations

AF	Acid fuchsine
ANA	acenaphthene
AOPs	advanced oxidation processes
ARS	Alizarin red S
BPA	Bisphenol-A
BR51	Basic Red 51
BSA	bovine serum albumin
BTEX	benzene, toluene, ethylbenzene, and xylene
CA	Clofibric acid
CB	Conduction bond
CBZ	carbamazepine
CeF	Cerium fluoride
CFX	Cefixime
CIP	Ciprofloxacin
CNCs	cellulose nanocrystals
COS	carbon oxidation state
DCF	diclofenac
MRs	Membrane reactors
MWCO	molecular weight cut-offs
MS	multiple sclerosis
NAP	naphthalene
NF	nanofiltration
PANI	Polyaniline
PCP	Pentachlorophenol
PdTFPP	(pentafluorophenyl)-21H, 23H-porphine palladium (II)
PE	polyethylene
PECM	photoelectrocatalytic membrane filtration
Penicillin G	Benzylpenicillin
PES	Polyethersulfone
PHE	phenanthrene
pHpzc	point of zero charge
PMRs	photocatalytic membrane reactors
PP	Polypropylene
PS	Phosphatidylserine

DCL	Diclofenac
DXM	Dexamethasone
E_a	band-gap energy
e^-_{CB}	conduction band electron
HPC	heterogeneous photocatalysis
hv	irradiated photons
h^+_{VB}	valence band hole
IBU	ibuprofen
IPMR	immobilized photocatalytic membrane reactors
MB	methylene blue
MF	microfiltration
MIL-53(Fe)	Matériaux de l'Institut Lavoisier
MNZ	Metronidazole
MO	Methyl Orange
MOF	Metal–organic framework
AF	Acid fuchsine
ANA	acenaphthene
AOPs	advanced oxidation processes
ARS	Alizarin red S
BPA	Bisphenol-A
BR51	Basic Red 51
BSA	bovine serum albumin
BTEX	benzene, toluene, ethylbenzene, and xylene
CA	Clofibric acid
CB	Conduction bond
CBZ	carbamazepine
CeF	Cerium fluoride
CFX	Cefixime
PVDF	polyvinylidene fluoride
RB5	Reactive Black 5
RO	Reverse osmosis
ROS	reactive oxygen species
SPMR	Suspended photocatalytic membrane reactors
TMP	transmembrane pressure
TPHs	total petroleum hydrocarbons
UF	ultrafiltration
UV	visible light
VB	Valance band
ZnONSt	zinc oxide nano stars
ZTPG	ZnO tetrapod-reduced graphene oxide

References

1. Chan, G.G.; Koch, C.M.; Connors, L.H. Blood proteomic profiling in inherited (ATTRm) and acquired (ATTRwt) forms of transthyretin-associated cardiac amyloidosis. *J. Proteome Res.* **2017**, *16*, 1659–1668.
2. Gligorovski, S.; Strekowski, R.; Barbati, S.; Vione, D. Environmental Implications of Hydroxyl Radicals (•OH). *Chem. Rev.* **2015**, *115*, 13051–13092. [CrossRef]
3. Doig, L.E.; Liber, K. An assessment of Hyalella azteca burrowing activity under laboratory sediment toxicity testing conditions. *Chemosphere* **2010**, *81*, 261–265.
4. Fereidooni, M.; Esmaeilzadeh, F.; Zandifar, A. Innovatively-synthesized CeO_2/ZnO photocatalysts by sono-photochemical deposition: Catalyst characterization and effect of operational parameters on high efficient dye removal. *J. Mater. Sci.* **2022**, *57*, 16228–16244. [CrossRef]
5. Reis, A.C.; Kolvenbach, B.A.; Nunes, O.C.; Corvini, P.F.X. Biodegradation of antibiotics: The new resistance determinants—Part II. *New Biotechnol.* **2020**, *54*, 13–27. [CrossRef]
6. Tian, Y.; Li, J.; Tang, L.; Meng, J.; Li, J. Antibiotics removal from piggery wastewater by a novel aerobic-microaerobic system: Efficiency and mechanism. *Chem. Eng. J.* **2023**, *454*, 140265. [CrossRef]
7. Barancheshme, F.; Munir, M. Strategies to Combat Antibiotic Resistance in the Wastewater Treatment Plants. *Front. Microbiol.* **2017**, *8*, 2603. [CrossRef]
8. Aguilar-Ascón, E.; Solari-Godiño, A.; Cueva-Martínez, M.; Neyra-Ascón, W.; Albrecht-Ruíz, M. Characterization of Sludge Resulting from Chemical Coagulation and Electrocoagulation of Pumping Water from Fishmeal Factories. *Processes* **2023**, *11*, 567.
9. Binazadeh, M.; Karimi, I.A.; Li, Z. Fast biodegradation of long chain n-alkanes and crude oil at high concentrations with *Rhodococcus* sp. Moj-3449. *Enzym. Microb. Technol.* **2009**, *45*, 195–202. [CrossRef]
10. Andreyev, S.Y.; Lebedinskiy, K.V.; Stepanov, S. A novel technology for optimizing dissolved air flotation unit efficiency via secondary saturation of the flotation cell with air bubbles and thin-layer settling. *Chem. Eng. Process.-Process Intensif.* **2023**, *184*, 109292.
11. Ahmad, A.; Priyadarshini, M.; Das, I.; Ghangrekar, M.M.; Surampalli, R.Y. Surfactant aided electrocoagulation/flotation using punched electrodes for the remediation of salicylic acid from wastewater. *J. Environ. Chem. Eng.* **2023**, *11*, 109049. [CrossRef]
12. Wysocka, I. Absorption processes in reducing the odor nuisance of wastewater. *MethodsX* **2023**, *10*, 101996. [CrossRef] [PubMed]
13. Rasouli, K.; Alamdari, A.; Sabbaghi, S. Ultrasonic-assisted synthesis of α-Fe_2O_3@ TiO_2 photocatalyst: Optimization of effective factors in the fabrication of photocatalyst and removal of non-biodegradable cefixime via response surface methodology-central composite design. *Sep. Purif. Technol.* **2023**, *307*, 122799. [CrossRef]

14. Kusworo, T.D.; Kumoro, A.C.; Aryanti, N.; Hasbullah, H.; Chaesarifa, D.R.S.; Fauzan, M.D.; Dalanta, F. Developing a robust photocatalytic and antifouling performance of PVDF membrane using spinel $NiFe_2O_4$/GO photocatalyst for efficient industrial dye wastewater treatment. *J. Environ. Chem. Eng.* **2023**, *11*, 109449. [CrossRef]
15. Binazadeh, M.; Li, Z.; Karimi, I.A. Optimization of biodegradation of long chain n-Alkanes by Rhodococcus sp. Moj-3449 using response surface methodology. *Phys. Chem. Res.* **2020**, *8*, 45–59.
16. Moradi, H.; Sabbaghi, S.; Mirbagheri, N.S.; Chen, P.; Rasouli, K.; Kamyab, H.; Chelliapan, S. Removal of chloride ion from drinking water using Ag NPs-Modified bentonite: Characterization and optimization of effective parameters by response surface methodology-central composite design. *Environ. Res.* **2023**, *223*, 115484. [CrossRef]
17. Molinari, R.; Lavorato, C.; Argurio, P.; Szymański, K.; Darowna, D.; Mozia, S. Overview of photocatalytic membrane reactors in organic synthesis, energy storage and environmental applications. *Catalysts* **2019**, *9*, 239. [CrossRef]
18. Pervez, M.N.; Talukder, M.E.; Mishu, M.R.; Buonerba, A.; Del Gaudio, P.; Stylios, G.K.; Hasan, S.W.; Zhao, Y.; Cai, Y.; Figoli, A.; et al. One-Step Fabrication of Novel Polyethersulfone-Based Composite Electrospun Nanofiber Membranes for Food Industry Wastewater Treatment. *Membranes* **2022**, *12*, 413. [CrossRef]
19. Koe, W.S.; Lee, J.W.; Chong, W.C.; Pang, Y.L.; Sim, L.C. An overview of photocatalytic degradation: Photocatalysts, mechanisms, and development of photocatalytic membrane. *Environ. Sci. Pollut. Res.* **2020**, *27*, 2522–2565. [CrossRef]
20. Khraibet, A.C.; Imran, N.J.; Majeed, H.M.; Ehmood, M.A.; Hasoon, G.S.; Nathim, Z.F.; Alwan, A.K.; Abd Alsada, A.S. Using titanium oxide membranes and ultraviolet (UV) light to remove pharmaceutical waste from hospitals wastewater. *J. Genet. Environ. Resour. Conserv.* **2022**, *10*, 41–48.
21. Sim, S.I.; Teow, Y.H. Integrated Membrane-adsorption system as a sustainable development approach for semiconductor-industry wastewater treatment. *Mater. Today Proc.* **2023**. [CrossRef]
22. Vasishta, A.; Mahale, J.S.; Pandey, P.H.; Ukarde, T.M.; Shinde, P.; Pawar, H.S. Membrane Separation: An Advanced Tool for the Development of a Wastewater Treatment Process. In *Membrane and Membrane-Based Processes for Wastewater Treatment*; CRC Press: Boca Raton, FL, USA, 2023; pp. 17–34.
23. Wu, J.; Wu, Y.; Hu, X.; Wu, C.; Ding, J. Water-bonding tubular membrane used in a 3D-printing dialyzer for diffusion dialysis. *J. Membr. Sci.* **2022**, *664*, 121078. [CrossRef]
24. Xie, J.; Yang, Y.; Zhang, H.; Chen, S.; Lv, Z.; Zhou, Y.; Qi, J.; Sun, X.; Li, J. ZIF-67 derived Co/N carbon hollow fiber membrane with excellent decontamination performance. *Chem. Eng. J.* **2023**, *451*, 138403. [CrossRef]
25. Dias, R.A.; Ferreira, R.S.B.; Medeiros, V.d.N.; Araujo, B.A.; Araújo, E.M.; Lira, H.d.L. Flat membranes of polyethersulfone/polysulfone blends in water/oil separation. *Polym. Bull.* **2022**, *80*, 4289–4305. [CrossRef]
26. Khalili, M.; Sabbaghi, S.; Zerafat, M.M. Preparation of ceramic γ-Al_2O_3–TiO_2 nanofiltration membranes for desalination. *Chem. Pap.* **2015**, *69*, 309–315. [CrossRef]
27. Baker, R.W. *Membrane Technology and Applications*; John Wiley & Sons: Hoboken, NJ, USA, 2012.
28. Pérez-Silva, I.; Páez-Hernández, M.; Ibarra, I.S.; Camacho-Mendoza, R.L. Evaluation of the Hybrid Membrane of ZnO Particles Supported in Cellulose Acetate for the Removal of Lead. *Membranes* **2023**, *13*, 123. [CrossRef] [PubMed]
29. Kayvani Fard, A.; McKay, G.; Buekenhoudt, A.; Al Sulaiti, H.; Motmans, F.; Khraisheh, M.; Atieh, M. Inorganic membranes: Preparation and application for water treatment and desalination. *Materials* **2018**, *11*, 74. [CrossRef]
30. Milovanovic, M.; Tabakoglu, F.; Saki, F.; Pohlkoetter, E.; Buga, D.; Brandt, V.; Tiller, J.C. Organic-inorganic double networks as highly permeable separation membranes with a chiral selector for organic solvents. *J. Membr. Sci.* **2023**, *668*, 121190. [CrossRef]
31. Darowna, D.; Wróbel, R.; Morawski, A.W.; Mozia, S. The influence of feed composition on fouling and stability of a polyethersulfone ultrafiltration membrane in a photocatalytic membrane reactor. *Chem. Eng. J.* **2017**, *310*, 360–367. [CrossRef]
32. Malekshahi, M.; Sabbaghi, S.; Rasouli, K. Preparation of α-alumina/γ-alumina/γ-alumina-titania ceramic composite membrane for chloride ion removal. *Mater. Chem. Phys.* **2022**, *287*, 126218. [CrossRef]
33. Pabby, A.K.; Rizvi, S.S.; Requena, A.M.S. *Handbook of Membrane Separations: Chemical, Pharmaceutical, Food, and Biotechnological Applications*; CRC Press: Boca Raton, FL, USA, 2008.
34. Mozia, S.; Rajakumaran, R.; Szymański, K.; Gryta, M. Removal of ketoprofen from surface water in a submerged photocatalytic membrane reactor utilizing membrane distillation: Effect of process parameters and evaluation of long-term performance. *J. Chem. Technol. Biotechnol.* **2023**. [CrossRef]
35. Feng, X.; Long, R.; Liu, C.; Liu, X. Novel dual-heterojunction photocatalytic membrane reactor based on Ag_2S/NH_2-MIL-88B (Fe)/poly (aryl ether nitrile) composite with enhanced photocatalytic performance for wastewater purification. *Chem. Eng. J.* **2023**, *454*, 139765. [CrossRef]
36. Molinari, R.; Limonti, C.; Lavorato, C.; Siciliano, A.; Argurio, P. Upgrade of a slurry photocatalytic membrane reactor based on a vertical filter and an external membrane and testing in the photodegradation of a model pollutant in water. *Chem. Eng. J.* **2023**, *451*, 138577. [CrossRef]
37. George, J.; Kumar, V.V. Designing a novel poly (methyl vinyl ether maleic anhydride) based polymeric membrane with enhanced antifouling performance for removal of pentachlorophenol from aqueous solution. *Environ. Res.* **2023**, *223*, 115404. [CrossRef] [PubMed]
38. Tian, S.; He, Y.; Zhang, L.; Li, S.; Bai, Y.; Wang, Y.; Wu, J.; Yu, J.; Guo, X. CNTs/TiO_2-loaded carbonized nanofibrous membrane with two-type self-cleaning performance for high efficiency oily wastewater remediation. *Colloids Surf. A Physicochem. Eng. Asp.* **2023**, *656*, 130306. [CrossRef]

39. Sisi, A.J.; Fathinia, M.; Khataee, A.; Orooji, Y. Systematic activation of potassium peroxydisulfate with ZIF-8 via sono-assisted catalytic process: Mechanism and ecotoxicological analysis. *J. Mol. Liq.* **2020**, *308*, 113018. [CrossRef]
40. Ghasemi, M.; Khataee, A.; Gholami, P.; Soltani, R.D.C.; Hassani, A.; Orooji, Y. In-situ electro-generation and activation of hydrogen peroxide using a CuFeNLDH-CNTs modified graphite cathode for degradation of cefazolin. *J. Environ. Manag.* **2020**, *267*, 110629. [CrossRef]
41. Sharma, K.; Vaya, D.; Prasad, G.; Surolia, P. Photocatalytic process for oily wastewater treatment: A review. *Int. J. Environ. Sci. Technol.* **2022**, *20*, 4615–4634. [CrossRef]
42. Chakachaka, V.; Tshangana, C.; Mahlangu, O.; Mamba, B.; Muleja, A. Interdependence of Kinetics and Fluid Dynamics in the Design of Photocatalytic Membrane Reactors. *Membranes* **2022**, *12*, 745. [CrossRef]
43. Hou, C.; Yuan, X.; Niu, M.; Li, Y.; Wang, L.; Zhang, M. In situ composite of Co-MOF on a Ti-based material for visible light multiphase catalysis: Synthesis and the photocatalytic degradation mechanism. *New J. Chem.* **2022**, *46*, 11341–11349. [CrossRef]
44. Wu, L.; Fu, C.; Huang, W. Surface chemistry of TiO_2 connecting thermal catalysis and photocatalysis. *Phys. Chem. Chem. Phys.* **2020**, *22*, 9875–9909. [CrossRef]
45. Zheng, X.; Shen, Z.-P.; Shi, L.; Cheng, R.; Yuan, D.-H. Photocatalytic membrane reactors (PMRs) in water treatment: Configurations and influencing factors. *Catalysts* **2017**, *7*, 224. [CrossRef]
46. Ensie, B.; Samad, S. Removal of nitrate from drinking water using nano SiO_2–FeOOH–Fe core–shell. *Desalination* **2014**, *347*, 1–9. [CrossRef]
47. Molinari, R.; Argurio, P.; Bellardita, M.; Palmisano, L.; Bertoni, C. Photocatalytic processes in membrane reactors. In *Comprehensive Membrane Science and Engineering*, 2nd ed.; Elsevier: Oxford, UK, 2017.
48. Vijayakumar, E.; Govinda Raj, M.; Narendran, M.G.; Preetha, R.; Mohankumar, R.; Neppolian, B.; John Bosco, A. Promoting Spatial Charge Transfer of ZrO_2 Nanoparticles: Embedded on Layered MoS_2/g-C_3N_4 Nanocomposites for Visible-Light-Induced Photocatalytic Removal of Tetracycline. *ACS Omega* **2022**, *7*, 5079–5095. [CrossRef]
49. Hardikar, M.; Marquez, I.; Achilli, A. Emerging investigator series: Membrane distillation and high salinity: Analysis and implications. *Environ. Sci. Water Res. Technol.* **2020**, *6*, 1538–1552. [CrossRef]
50. Aliyu, U.M.; Rathilal, S.; Isa, Y.M. Membrane desalination technologies in water treatment: A review. *Water Pract. Technol.* **2018**, *13*, 738–752. [CrossRef]
51. Rao, L.; Tang, J.; Hu, S.; Shen, L.; Xu, Y.; Li, R.; Lin, H. Inkjet printing assisted electroless Ni plating to fabricate nickel coated polypropylene membrane with improved performance. *J. Colloid Interface Sci.* **2020**, *565*, 546–554. [CrossRef]
52. Hassanzadeh, E.; Farhadian, M.; Razmjou, A.; Askari, N. An efficient wastewater treatment approach for a real woolen textile industry using a chemical assisted NF membrane process. *Environ. Nanotechnol. Monit. Manag.* **2017**, *8*, 92–96. [CrossRef]
53. Wang, L.; Liang, W.; Chen, W.; Zhang, W.; Mo, J.; Liang, K.; Tang, B.; Zheng, Y.; Jiang, F. Integrated aerobic granular sludge and membrane process for enabling municipal wastewater treatment and reuse water production. *Chem. Eng. J.* **2018**, *337*, 300–311. [CrossRef]
54. Alardhi, S.M.; Albayati, T.M.; Alrubaye, J.M. A hybrid adsorption membrane process for removal of dye from synthetic and actual wastewater. *Chem. Eng. Process.-Process Intensif.* **2020**, *157*, 108113. [CrossRef]
55. Yun, T.; Chung, J.W.; Kwak, S.-Y. Recovery of sulfuric acid aqueous solution from copper-refining sulfuric acid wastewater using nanofiltration membrane process. *J. Environ. Manag.* **2018**, *223*, 652–657. [CrossRef] [PubMed]
56. Mir, M.A.; Bhat, M.A.; Majid, S.A.; Lone, S.H.; Malla, M.A.; Tiwari, K.R.; Pandit, A.H.; Tomar, R.; Bhat, R.A. Studies on the synthesis and characterization of polyaniline-zeolite nanostructures and their role in carbon monoxide sensing. *J. Environ. Chem. Eng.* **2018**, *6*, 1137–1146.
57. Ren, Q.; Chen, X.; Yumminaga, Y.; Wang, N.; Yan, W.; Li, Y.; Liu, L.; Shi, J. Effect of operating conditions on the performance of multichannel ceramic ultrafiltration membranes for cattle wastewater treatment. *J. Water Process Eng.* **2021**, *41*, 102102. [CrossRef]
58. Belibagli, P.; Isik, Z.; Özdemir, S.; Gonca, S.; Dizge, N.; Awasthi, M.K.; Balakrishnan, D. An integrated process for wet scrubber wastewater treatment using electrooxidation and pressure-driven membrane filtration. *Chemosphere* **2022**, *308*, 136216. [CrossRef] [PubMed]
59. Sathya, U.; Nithya, M.; Balasubramanian, N. Evaluation of advanced oxidation processes (AOPs) integrated membrane bioreactor (MBR) for the real textile wastewater treatment. *J. Environ. Manag.* **2019**, *246*, 768–775. [CrossRef] [PubMed]
60. Tang, Y.; Lin, Y.; Ford, D.M.; Qian, X.; Cervellere, M.R.; Millett, P.C.; Wang, X. A review on models and simulations of membrane formation via phase inversion processes. *J. Membr. Sci.* **2021**, *640*, 119810. [CrossRef]
61. Wang, Y.; Li, T.; Zhu, J. Study on treatment of wastewater with low concentration of ammonia-nitrogen by vacuum plate membrane distillation technology. *Water Sci. Technol.* **2022**, *86*, 950–967. [CrossRef]
62. Al-Juboori, R.A.; Naji, O.; Bowtell, L.; Alpatova, A.; Soukane, S.; Ghaffour, N. Power effect of ultrasonically vibrated spacers in air gap membrane distillation: Theoretical and experimental investigations. *Sep. Purif. Technol.* **2021**, *262*, 118319. [CrossRef]
63. Kubo, M.; Kojima, M.; Mano, R.; Daiko, Y.; Honda, S.; Iwamoto, Y. A hydrostable mesoporous γ-Al_2O_3 membrane modified with Si–C–H organic-inorganic hybrid derived from polycarbosilane. *J. Membr. Sci.* **2020**, *598*, 117799. [CrossRef]
64. Abd Jalil, S.N. Investigation of Vacuum-Assisted Preparation Methods of Inorganic Membranes. Master's Thesis, School of Chemical Engineering, The University of Queensland, St Lucia, QLD, Australia, 2017.
65. Mamivand, S.; Binazadeh, M.; Sohrabi, R. Applicability of membrane reactor technology in industrial hydrogen producing reactions: Current effort and future directions. *J. Ind. Eng. Chem.* **2021**, *104*, 212–230. [CrossRef]

66. Khan, A.; Khan, S.J.; Miran, W.; Zaman, W.Q.; Aslam, A.; Shahzad, H.M.A. Feasibility Study of Anaerobic Baffled Reactor Coupled with Anaerobic Filter Followed by Membrane Filtration for Wastewater Treatment. *Membranes* **2023**, *13*, 79. [CrossRef] [PubMed]
67. Jang, D.; Lee, J.; Jang, A. Impact of pre-coagulation on the ceramic membrane process during oil-water emulsion separation: Fouling behavior and mechanism. *Chemosphere* **2023**, *313*, 137596. [CrossRef] [PubMed]
68. Ghalamchi, L.; Aber, S.; Vatanpour, V.; Kian, M. Comparison of NLDH and g-C_3N_4 nanoplates and formative Ag_3PO_4 nanoparticles in PES microfiltration membrane fouling: Applications in MBR. *Chem. Eng. Res. Des.* **2019**, *147*, 443–457. [CrossRef]
69. Shahabi, S.S.; Azizi, N.; Vatanpour, V. Synthesis and characterization of novel g-C_3N_4 modified thin film nanocomposite reverse osmosis membranes to enhance desalination performance and fouling resistance. *Sep. Purif. Technol.* **2019**, *215*, 430–440. [CrossRef]
70. Turgut, F.; Chong, C.Y.; Karaman, M.; Lau, W.J.; Gürsoy, M.; Ismail, A.F. Plasma surface modification of graphene oxide nanosheets for the synthesis of GO/PES nanocomposite ultrafiltration membrane for enhanced oily separation. *J. Appl. Polym. Sci.* **2023**, *140*, e53410. [CrossRef]
71. Goh, P.S.; Samavati, Z.; Ismail, A.F.; Ng, B.C.; Abdullah, M.S.; Hilal, N. Modification of Liquid Separation Membranes Using Multidimensional Nanomaterials: Revealing the Roles of Dimension Based on Classical Titanium Dioxide. *Nanomaterials* **2023**, *13*, 448. [CrossRef]
72. Bera, S.P.; Godhaniya, M.; Kothari, C. Emerging and advanced membrane technology for wastewater treatment: A review. *J. Basic Microbiol.* **2022**, *62*, 245–259. [CrossRef]
73. Shehata, N.; Egirani, D.; Olabi, A.; Inayat, A.; Abdelkareem, M.A.; Chae, K.-J.; Sayed, E.T. Membrane-based water and wastewater treatment technologies: Issues, current trends, challenges, and role in achieving sustainable development goals, and circular economy. *Chemosphere* **2023**, *320*, 137993.
74. Hyeon, Y.; Kim, S.; Ok, E.; Park, C. A fluid imaging flow cytometry for rapid characterization and realistic evaluation of microplastic fiber transport in ceramic membranes for laundry wastewater treatment. *Chem. Eng. J.* **2023**, *454*, 140028. [CrossRef]
75. Huang, S.; Wu, G.; Chen, S. Preparation of microporous poly (vinylidene fluoride) membranes via phase inversion in supercritical CO_2. *J. Membr. Sci.* **2007**, *293*, 100–110. [CrossRef]
76. Kim, N.; Kim, C.-S.; Lee, Y.-T. Preparation and characterization of polyethersulfone membranes with p-toluenesulfonic acid and polyvinylpyrrolidone additives. *Desalination* **2008**, *233*, 218–226. [CrossRef]
77. Lee, A.; Elam, J.W.; Darling, S.B. Membrane materials for water purification: Design, development, and application. *Environ. Sci. Water Res. Technol.* **2016**, *2*, 17–42. [CrossRef]
78. Zikalala, S.A.; Chabalala, M.B.; Gumbi, N.N.; Coville, N.J.; Mamba, B.B.; Mutuma, B.K.; Nxumalo, E.N. Microwave-assisted synthesis of titania–amorphous carbon nanotubes/amorphous nitrogen-doped carbon nanotubes nanohybrids for photocatalytic degradation of textile wastewater. *RSC Adv.* **2021**, *11*, 6748–6763. [CrossRef] [PubMed]
79. Szymański, K.; Gryta, M.; Darowna, D.; Mozia, S. A new submerged photocatalytic membrane reactor based on membrane distillation for ketoprofen removal from various aqueous matrices. *Chem. Eng. J.* **2022**, *435*, 134872. [CrossRef]
80. Gupta, S.; Gomaa, H.; Ray, M.B. Fouling control in a submerged membrane reactor: Aeration vs. membrane oscillations. *Chem. Eng. J.* **2022**, *432*, 134399. [CrossRef]
81. Ganiyu, S.O.; Van Hullebusch, E.D.; Cretin, M.; Esposito, G.; Oturan, M.A. Coupling of membrane filtration and advanced oxidation processes for removal of pharmaceutical residues: A critical review. *Sep. Purif. Technol.* **2015**, *156*, 891–914. [CrossRef]
82. Hu, C.; Wang, M.-S.; Chen, C.-H.; Chen, Y.-R.; Huang, P.-H.; Tung, K.-L. Phosphorus-doped g-C_3N_4 integrated photocatalytic membrane reactor for wastewater treatment. *J. Membr. Sci.* **2019**, *580*, 1–11. [CrossRef]
83. Vickers, J. Animal communication: When I'm calling you, will you answer too? *Curr. Biol.* **2017**, *27*, R713–R715.
84. Nguyen, V.-H.; Tran, Q.B.; Nguyen, X.C.; Hai, L.T.; Ho, T.T.T.; Shokouhimehr, M.; Vo, D.-V.N.; Lam, S.S.; Nguyen, H.P.; Hoang, C.T.; et al. Submerged photocatalytic membrane reactor with suspended and immobilized N-doped TiO_2 under visible irradiation for diclofenac removal from wastewater. *Process Saf. Environ. Prot.* **2020**, *142*, 229–237. [CrossRef]
85. Kemp, K.; Griffiths, J.; Campbell, S.; Lovell, K. An exploration of the follow-up up needs of patients with inflammatory bowel disease. *J. Crohn's Colitis* **2013**, *7*, e386–e395.
86. Espíndola, J.C.; Cristóvão, R.O.; Mendes, A.; Boaventura, R.A.R.; Vilar, V.J.P. Photocatalytic membrane reactor performance towards oxytetracycline removal from synthetic and real matrices: Suspended vs. immobilized TiO_2-P25. *Chem. Eng. J.* **2019**, *378*, 122114. [CrossRef]
87. Salehian, S.; Heydari, H.; Khansanami, M.; Vatanpour, V.; Mousavi, S.A. Fabrication and performance of polysulfone/H_2O_2-g-C_3N_4 mixed matrix membrane in a photocatalytic membrane reactor under visible light irradiation for removal of natural organic matter. *Sep. Purif. Technol.* **2022**, *285*, 120291. [CrossRef]
88. Ahmadi, A.; Sarrafzadeh, M.-H.; Hosseinian, A.; Ghaffari, S.-B. Foulant layer degradation of dye in Photocatalytic Membrane Reactor (PMR) containing immobilized and suspended NH_2-MIL125(Ti) MOF led to water flux recovery. *J. Environ. Chem. Eng.* **2022**, *10*, 106999. [CrossRef]
89. Rathna, T.; PonnanEttiyappan, J.; RubenSudhakar, D. Fabrication of visible-light assisted TiO_2-WO_3-PANI membrane for effective reduction of chromium (VI) in photocatalytic membrane reactor. *Environ. Technol. Innov.* **2021**, *24*, 102023. [CrossRef]
90. Petsi, P.N.; Sarasidis, V.C.; Plakas, K.V.; Karabelas, A.J. Reduction of nitrates in a photocatalytic membrane reactor in the presence of organic acids. *J. Environ. Manag.* **2021**, *298*, 113526. [CrossRef] [PubMed]

91. Azimifar, M.; Ghorbani, M.; Peyravi, M. Fabrication and evaluation of a photocatalytic membrane based on Sb_2O_3/CBO composite for improvement of dye removal efficiency. *J. Mol. Struct.* **2022**, *1270*, 133957. [CrossRef]
92. Hindryawati, N.; Maniam, G.P.; Pratama, I.R.; Gunawan, R.; Koesnarpadi, S. Study of Sonocatalytic Activity ZnO-WO_3 Composite on Degradation Phenol in Aqueous Solution. *J. Bahan Alam Terbarukan* **2022**, *11*, 50–57. [CrossRef]
93. Fujishima, A.; Honda, K. Electrochemical photolysis of water at a semiconductor electrode. *Nature* **1972**, *238*, 37–38. [CrossRef]
94. Zhang, J.; Tian, B.; Wang, L.; Xing, M.; Lei, J. Mechanism of photocatalysis. In *Photocatalysis*; Springer: Berlin/Heidelberg, Germany, 2018; pp. 1–15.
95. Khalid, N.; Majid, A.; Tahir, M.B.; Niaz, N.; Khalid, S. Carbonaceous-TiO_2 nanomaterials for photocatalytic degradation of pollutants: A review. *Ceram. Int.* **2017**, *43*, 14552–14571. [CrossRef]
96. Nair, V.; Muñoz-Batista, M.J.; Fernández-García, M.; Luque, R.; Colmenares, J.C. Thermo-photocatalysis: Environmental and energy applications. *ChemSusChem* **2019**, *12*, 2098–2116. [CrossRef]
97. Zyoud, A.H.; Zubi, A.; Hejjawi, S.; Zyoud, S.H.; Helal, M.H.; Zyoud, S.H.; Qamhieh, N.; Hajamohideen, A.; Hilal, H.S. Removal of acetaminophen from water by simulated solar light photodegradation with ZnO and TiO_2 nanoparticles: Catalytic efficiency assessment for future prospects. *J. Environ. Chem. Eng.* **2020**, *8*, 104038. [CrossRef]
98. Sabouni, R.; Gomaa, H. Photocatalytic degradation of pharmaceutical micro-pollutants using ZnO. *Environ. Sci. Pollut. Res.* **2019**, *26*, 5372–5380. [CrossRef] [PubMed]
99. Saha, M.S.; Li, R.; Sun, X. High loading and monodispersed Pt nanoparticles on multiwalled carbon nanotubes for high performance proton exchange membrane fuel cells. *J. Power Sources* **2008**, *177*, 314–322.
100. Guo, Q.; Tang, G.; Zhu, W.; Luo, Y.; Gao, X. In situ construction of Z-scheme FeS_2/Fe_2O_3 photocatalyst via structural transformation of pyrite for photocatalytic degradation of carbamazepine and the synergistic reduction of Cr (VI). *J. Environ. Sci.* **2021**, *101*, 351–360. [CrossRef] [PubMed]
101. Berkani, M.; Smaali, A.; Kadmi, Y.; Almomani, F.; Vasseghian, Y.; Lakhdari, N.; Alyane, M. Photocatalytic degradation of Penicillin G in aqueous solutions: Kinetic, degradation pathway, and microbioassays assessment. *J. Hazard. Mater.* **2022**, *421*, 126719. [CrossRef]
102. Arghavan, F.S.; Hossein Panahi, A.; Nasseh, N.; Ghadirian, M. Adsorption-photocatalytic processes for removal of pentachlorophenol contaminant using $FeNi_3$/SiO_2/ZnO magnetic nanocomposite under simulated solar light irradiation. *Environ. Sci. Pollut. Res.* **2021**, *28*, 7462–7475. [CrossRef]
103. Eskandari, M.; Goudarzi, N.; Moussavi, S.G. Application of low-voltage UVC light and synthetic ZnO nanoparticles to photocatalytic degradation of ciprofloxacin in aqueous sample solutions. *Water Environ. J.* **2018**, *32*, 58–66. [CrossRef]
104. Bohdziewicz, J.; Kudlek, E.; Dudziak, M. Influence of the catalyst type (TiO_2 and ZnO) on the photocatalytic oxidation of pharmaceuticals in the aquatic environment. *Desalination Water Treat.* **2016**, *57*, 1552–1563. [CrossRef]
105. Beheshti, F.; Tehrani, R.M.A.; Khadir, A. Sulfamethoxazole removal by photocatalytic degradation utilizing TiO_2 and WO_3 nanoparticles as catalysts: Analysis of various operational parameters. *Int. J. Environ. Sci. Technol.* **2019**, *16*, 7987–7996. [CrossRef]
106. Ghenaatgar, A.; Tehrani, R.M.; Khadir, A. Photocatalytic degradation and mineralization of dexamethasone using WO_3 and ZrO_2 nanoparticles: Optimization of operational parameters and kinetic studies. *J. Water Process Eng.* **2019**, *32*, 100969. [CrossRef]
107. Farzadkia, M.; Bazrafshan, E.; Esrafili, A.; Yang, J.-K.; Shirzad-Siboni, M. Photocatalytic degradation of Metronidazole with illuminated TiO_2 nanoparticles. *J. Environ. Health Sci. Eng.* **2015**, *13*, 35. [CrossRef]
108. Heidari, S.; Haghighi, M.; Shabani, M. Sunlight-activated BiOCl/BiOBr–$Bi_{24}O_{31}Br_{10}$ photocatalyst for the removal of pharmaceutical compounds. *J. Clean. Prod.* **2020**, *259*, 120679. [CrossRef]
109. Chinnaiyan, P.; Thampi, S.; Kumar, M.; Balachandran, M. Photocatalytic degradation of metformin and amoxicillin in synthetic hospital wastewater: Effect of classical parameters. *Int. J. Environ. Sci. Technol.* **2019**, *16*, 5463–5474. [CrossRef]
110. Thi, V.H.-T.; Lee, B.-K. Effective photocatalytic degradation of paracetamol using La-doped ZnO photocatalyst under visible light irradiation. *Mater. Res. Bull.* **2017**, *96*, 171–182. [CrossRef]
111. Salehia, F.; Sabbaghia, S.; Mirbagherib, N.S. Modification of graphitic carbon nitride photocatalyst by Pb-contaminated water for efficient removal of cefixime from aqueous media. *Desalination Water Treat.* **2021**, *229*, 331–342. [CrossRef]
112. Cruz, D.; Ortiz-Oliveros, H.B.; Flores-Espinosa, R.M.; Ávila Pérez, P.; Ruiz-López, I.I.; Quiroz-Estrada, K.F. Synthesis of Ag/TiO_2 composites by combustion modified and subsequent use in the photocatalytic degradation of dyes. *J. King Saud Univ.-Sci.* **2022**, *34*, 101966. [CrossRef]
113. Sima, J.; Hasal, P. Photocatalytic degradation of textile dyes in a TiO_2/UV system. *Chem. Eng. Trans.* **2013**, *32*, 79–84.
114. Kumaresan, A.; Arun, A.; Kalpana, V.; Vinupritha, P.; Sundaravadivel, E. Polymer-supported $NiWO_4$ nanocomposites for visible light degradation of toxic dyes. *J. Mater. Sci. Mater. Electron.* **2022**, *33*, 9660–9668. [CrossRef]
115. Ye, Z.; Kong, L.; Chen, F.; Chen, Z.; Lin, Y.; Liu, C. A comparative study of photocatalytic activity of ZnS photocatalyst for degradation of various dyes. *Optik* **2018**, *164*, 345–354. [CrossRef]
116. Shi, J.; Zheng, J.; Wu, P.; Ji, X. Immobilization of TiO_2 films on activated carbon fiber and their photocatalytic degradation properties for dye compounds with different molecular size. *Catal. Commun.* **2008**, *9*, 1846–1850. [CrossRef]
117. Kumar, S.; Kaushik, R.; Purohit, L. Novel ZnO tetrapod-reduced graphene oxide nanocomposites for enhanced photocatalytic degradation of phenolic compounds and MB dye. *J. Mol. Liq.* **2021**, *327*, 114814. [CrossRef]
118. Yashni, G.; AlGheethi, A.; Mohamed, R.M.S.R.; Arifin, S.N.H.; Shanmugan, V.A.; Kassim, A.H.M. Photocatalytic degradation of basic red 51 dye in artificial bathroom greywater using zinc oxide nanoparticles. *Mater. Today Proc.* **2020**, *31*, 136–139. [CrossRef]

119. Ameen, F.; Dawoud, T.; AlNadhari, S. Ecofriendly and low-cost synthesis of ZnO nanoparticles from Acremonium potronii for the photocatalytic degradation of azo dyes. *Environ. Res.* **2021**, *202*, 111700. [CrossRef] [PubMed]
120. Arikal, D.; Kallingal, A. Photocatalytic degradation of azo and anthraquinone dye using TiO_2/MgO nanocomposite immobilized chitosan hydrogels. *Environ. Technol.* **2021**, *42*, 2278–2291. [CrossRef]
121. Zeng, Q.; Liu, Y.; Shen, L.; Lin, H.; Yu, W.; Xu, Y.; Li, R.; Huang, L. Facile preparation of recyclable magnetic Ni@ filter paper composite materials for efficient photocatalytic degradation of methyl orange. *J. Colloid Interface Sci.* **2021**, *582*, 291–300. [CrossRef] [PubMed]
122. de Jesus Cubas, P.; Semkiw, A.W.; Monteiro, F.C.; Los Weinert, P.; Monteiro, J.F.H.L.; Fujiwara, S.T. Synthesis of $CuCr_2O_4$ by self-combustion method and photocatalytic activity in the degradation of Azo Dye with visible light. *J. Photochem. Photobiol. A Chem.* **2020**, *401*, 112797. [CrossRef]
123. Aziz, A.; Ali, N.; Khan, A.; Bilal, M.; Malik, S.; Ali, N.; Khan, H. Chitosan-zinc sulfide nanoparticles, characterization and their photocatalytic degradation efficiency for azo dyes. *Int. J. Biol. Macromol.* **2020**, *153*, 502–512. [CrossRef]
124. El Nahrawy, A.M.; Abou Hammad, A.B.; Bakr, A.M.; Hemdan, B.A.; Wassel, A.R. Decontamination of ubiquitous harmful microbial lineages in water using an innovative $Zn_2Ti_{0.8}Fe_{0.2}O_4$ nanostructure: Dielectric and terahertz properties. *Heliyon* **2019**, *5*, e02501. [CrossRef]
125. Guo, N.; Zeng, Y.; Li, H.; Xu, X.; Yu, H.; Han, X. Novel mesoporous TiO_2@ g-C_3N_4 hollow core@ shell heterojunction with enhanced photocatalytic activity for water treatment and H_2 production under simulated sunlight. *J. Hazard. Mater.* **2018**, *353*, 80–88. [CrossRef]
126. Mohsenzadeh, M.; Mirbagheri, S.A.; Sabbaghi, S. Degradation of 1,2-dichloroethane by photocatalysis using immobilized PAni-TiO_2 nano-photocatalyst. *Environ. Sci. Pollut. Res.* **2019**, *26*, 31328–31343. [CrossRef]
127. Schnabel, T.; Jautzus, N.; Mehling, S.; Springer, C.; Londong, J. Photocatalytic degradation of hydrocarbons and methylene blue using floatable titanium dioxide catalysts in contaminated water. *J. Water Reuse Desalination* **2021**, *11*, 224–235. [CrossRef]
128. Rani, C.N.; Karthikeyan, S. Synergic effects on degradation of a mixture of polycyclic aromatic hydrocarbons in a UV slurry photocatalytic membrane reactor and its cost estimation. *Chem. Eng. Process.-Process Intensif.* **2021**, *159*, 108179. [CrossRef]
129. Mousavi, S.M.; Hashemi, S.A.; Zarei, M.; Bahrani, S.; Savardashtaki, A.; Esmaeili, H.; Lai, C.W.; Mazraedoost, S.; Abassi, M.; Ramavandi, B. Data on cytotoxic and antibacterial activity of synthesized Fe_3O_4 nanoparticles using Malva sylvestris. *Data Brief* **2020**, *28*, 104929. [CrossRef] [PubMed]
130. Ul Haq, I.; Ahmad, W.; Ahmad, I.; Yaseen, M. Photocatalytic oxidative degradation of hydrocarbon pollutants in refinery wastewater using TiO_2 as catalyst. *Water Environ. Res.* **2020**, *92*, 2086–2094. [CrossRef] [PubMed]
131. Rahmani, E.; Rahmani, M.; Silab, H.R. TiO_2: SiO_2 thin film coated annular photoreactor for degradation of oily contamination from waste water. *J. Water Process Eng.* **2020**, *37*, 101374. [CrossRef]
132. Cho, I.H.; Kim, L.H.; Zoh, K.D.; Park, J.H.; Kim, H.Y. Solar photocatalytic degradation of groundwater contaminated with petroleum hydrocarbons. *Environ. Prog.* **2006**, *25*, 99–109. [CrossRef]
133. Mukwevho, N.; Gusain, R.; Fosso-Kankeu, E.; Kumar, N.; Waanders, F.; Ray, S.S. Removal of naphthalene from simulated wastewater through adsorption-photodegradation by ZnO/Ag/GO nanocomposite. *J. Ind. Eng. Chem.* **2020**, *81*, 393–404. [CrossRef]
134. Sheikholeslami, Z.; Yousefi Kebria, D.; Qaderi, F. Investigation of photocatalytic degradation of BTEX in produced water using γ-Fe_2O_3 nanoparticle. *J. Therm. Anal. Calorim.* **2019**, *135*, 1617–1627. [CrossRef]
135. Sekar, A.D.; Muthukumar, H.; Chandrasekaran, N.I.; Matheswaran, M. Photocatalytic degradation of naphthalene using calcined FeZnO/PVA nanofibers. *Chemosphere* **2018**, *205*, 610–617. [CrossRef]
136. Rani, M.; Shanker, U. Enhanced photocatalytic degradation of chrysene by Fe_2O_3@ ZnHCF nanocubes. *Chem. Eng. J.* **2018**, *348*, 754–764.
137. Tiburtius, E.R.L.; Peralta-Zamora, P.; Emmel, A. Treatment of gasoline-contaminated waters by advanced oxidation processes. *J. Hazard. Mater.* **2005**, *126*, 86–90. [CrossRef] [PubMed]
138. Mohammadifard, Z.; Saboori, R.; Mirbagheri, N.S.; Sabbaghi, S. Heterogeneous photo-Fenton degradation of formaldehyde using MIL-100(Fe) under visible light irradiation. *Environ. Pollut.* **2019**, *251*, 783–791. [CrossRef] [PubMed]
139. Veerakumar, P.; Sangili, A.; Saranya, K.; Pandikumar, A.; Lin, K.-C. Palladium and silver nanoparticles embedded on zinc oxide nanostars for photocatalytic degradation of pesticides and herbicides. *Chem. Eng. J.* **2021**, *410*, 128434. [CrossRef]
140. Cavalcante, R.P.; de Oliveira, D.M.; da Silva, L.d.M.; Giménez, J.; Esplugas, S.; de Oliveira, S.C.; Dantas, R.F.; Sans, C.; Machulek, A. Evaluation of the main active species involved in the TiO_2 photocatalytic degradation of ametryn herbicide and its by-products. *J. Environ. Chem. Eng.* **2021**, *9*, 105109. [CrossRef]
141. Samsudin, M.F.R.; Jayabalan, P.J.; Ong, W.-J.; Ng, Y.H.; Sufian, S. Photocatalytic degradation of real industrial poultry wastewater via platinum decorated $BiVO_4$/g-C_3N_4 photocatalyst under solar light irradiation. *J. Photochem. Photobiol. A Chem.* **2019**, *378*, 46–56. [CrossRef]
142. Rani, M.; Shanker, U. Efficient photocatalytic degradation of Bisphenol A by metal ferrites nanoparticles under sunlight. *Environ. Technol. Innov.* **2020**, *19*, 100792. [CrossRef]
143. Tsoumachidou, S.; Velegraki, T.; Poulios, I. TiO_2 photocatalytic degradation of UV filter para-aminobenzoic acid under artificial and solar illumination. *J. Chem. Technol. Biotechnol.* **2016**, *91*, 1773–1781. [CrossRef]

144. Kangralkar, M.V.; Manjanna, J.; Momin, N.; Rane, K.; Nayaka, G.; Kangralkar, V.A. Photocatalytic degradation of hexavalent chromium and different staining dyes by ZnO in aqueous medium under UV light. *Environ. Nanotechnol. Monit. Manag.* **2021**, *16*, 100508. [CrossRef]
145. Santhosh, C.; Malathi, A.; Daneshvar, E.; Kollu, P.; Bhatnagar, A. Photocatalytic degradation of toxic aquatic pollutants by novel magnetic 3D-TiO_2@ HPGA nanocomposite. *Sci. Rep.* **2018**, *8*, 15531. [CrossRef]
146. Chen, P.; Wang, F.; Zhang, Q.; Su, Y.; Shen, L.; Yao, K.; Chen, Z.-F.; Liu, Y.; Cai, Z.; Lv, W. Photocatalytic degradation of clofibric acid by g-C_3N_4/P25 composites under simulated sunlight irradiation: The significant effects of reactive species. *Chemosphere* **2017**, *172*, 193–200. [CrossRef]
147. Truc, N.T.T.; Duc, D.S.; Van Thuan, D.; Al Tahtamouni, T.; Pham, T.-D.; Hanh, N.T.; Tran, D.T.; Nguyen, M.V.; Dang, N.M.; Le Chi, N.T.P. The advanced photocatalytic degradation of atrazine by direct Z-scheme Cu doped ZnO/g-C_3N_4. *Appl. Surf. Sci.* **2019**, *489*, 875–882. [CrossRef]
148. Aoudj, S.; Khelifa, A.; Drouiche, N.; Belkada, R.; Miroud, D. Simultaneous removal of chromium (VI) and fluoride by electrocoagulation–electroflotation: Application of a hybrid Fe-Al anode. *Chem. Eng. J.* **2015**, *267*, 153–162. [CrossRef]
149. Kesarla, M.K.; Fuentez-Torres, M.O.; Alcudia-Ramos, M.A.; Ortiz-Chi, F.; Espinosa-González, C.G.; Aleman, M.; Torres-Torres, J.G.; Godavarthi, S. Synthesis of g-C_3N_4/N-doped CeO_2 composite for photocatalytic degradation of an herbicide. *J. Mater. Res. Technol.* **2019**, *8*, 1628–1635. [CrossRef]
150. Wongcharoen, S.; Panomsuwan, G. Easy synthesis of TiO_2 hollow fibers using kapok as a biotemplate for photocatalytic degradation of the herbicide paraquat. *Mater. Lett.* **2018**, *228*, 482–485. [CrossRef]
151. Mansourian, R.; Mousavi, S.M.; Alizadeh, S.; Sabbaghi, S. CeO_2/TiO_2/SiO_2 nanocatalyst for the photocatalytic and sonophotocatalytic degradation of chlorpyrifos. *Can. J. Chem. Eng.* **2022**, *100*, 451–464. [CrossRef]
152. Song, H.; Shao, J.; He, Y.; Liu, B.; Zhong, X. Natural organic matter removal and flux decline with PEG–TiO_2-doped PVDF membranes by integration of ultrafiltration with photocatalysis. *J. Membr. Sci.* **2012**, *405*, 48–56. [CrossRef]
153. Wang, F.; Chen, Z.; Zhu, Z.; Guo, J. Construction of visible light responsive ZnO/N-g-C_3N_4 composite membranes for antibiotics degradation. *J. Mater. Res. Technol.* **2022**, *17*, 1696–1706. [CrossRef]
154. Athanasekou, C.P.; Moustakas, N.G.; Morales-Torres, S.; Pastrana-Martínez, L.M.; Figueiredo, J.L.; Faria, J.L.; Silva, A.M.; Dona-Rodriguez, J.M.; Romanos, G.E.; Falaras, P. Ceramic photocatalytic membranes for water filtration under UV and visible light. *Appl. Catal. B Environ.* **2015**, *178*, 12–19. [CrossRef]
155. Chen, D.; Cheng, Y.; Zhou, N.; Chen, P.; Wang, Y.; Li, K.; Huo, S.; Cheng, P.; Peng, P.; Zhang, R. Photocatalytic degradation of organic pollutants using TiO_2-based photocatalysts: A review. *J. Clean. Prod.* **2020**, *268*, 121725. [CrossRef]
156. Ahmad, R.; Lee, C.S.; Kim, J.H.; Kim, J. Partially coated TiO_2 on Al_2O_3 membrane for high water flux and photodegradation by novel filtration strategy in photocatalytic membrane reactors. *Chem. Eng. Res. Des.* **2020**, *163*, 138–148. [CrossRef]
157. Wang, F.; Xu, J.; Wang, Z.; Lou, Y.; Pan, C.; Zhu, Y. Unprecedentedly efficient mineralization performance of photocatalysis-self-Fenton system towards organic pollutants over oxygen-doped porous g-C_3N_4 nanosheets. *Appl. Catal. B Environ.* **2022**, *312*, 121438. [CrossRef]
158. Čizmić, M.; Ljubas, D.; Rožman, M.; Ašperger, D.; Ćurković, L.; Babić, S. Photocatalytic degradation of azithromycin by nanostructured TiO_2 film: Kinetics, degradation products, and toxicity. *Materials* **2019**, *12*, 873. [CrossRef] [PubMed]
159. Shang, C.; Bu, J.; Song, C. Preparation, Antimicrobial Properties under Different Light Sources, Mechanisms and Applications of TiO_2: A Review. *Materials* **2022**, *15*, 5820. [CrossRef]
160. Singh, A.; Ramachandran, S.K.; Gumpu, M.B.; Zsuzsanna, L.; Veréb, G.; Kertész, S.; Gangasalam, A. Titanium dioxide doped hydroxyapatite incorporated photocatalytic membranes for the degradation of chloramphenicol antibiotic in water. *J. Chem. Technol. Biotechnol.* **2020**, *96*, 1057–1066. [CrossRef]
161. Zakeritabar, S.F.; Jahanshahi, M.; Peyravi, M.; Akhtari, J. Photocatalytic study of nanocomposite membrane modified by CeF_3 catalyst for pharmaceutical wastewater treatment. *J. Environ. Health Sci. Eng.* **2020**, *18*, 1151–1161. [CrossRef] [PubMed]
162. Shaku, K.; Dlamini, L.; Malinga, S. Highly efficient photocatalytic hyperbranched polyethyleneimine/bismuth vanadate membranes for the degradation of triclosan. *Int. J. Environ. Sci. Technol.* **2020**, *17*, 3297–3312. [CrossRef]
163. Yu, S.; Wang, Y.; Sun, F.; Wang, R.; Zhou, Y. Novel mpg-C_3N_4/TiO_2 nanocomposite photocatalytic membrane reactor for sulfamethoxazole photodegradation. *Chem. Eng. J.* **2018**, *337*, 183–192. [CrossRef]
164. Sun, S.; Yao, H.; Fu, W.; Xue, S.; Zhang, W. Enhanced degradation of antibiotics by photo-fenton reactive membrane filtration. *J. Hazard. Mater.* **2020**, *386*, 121955. [CrossRef]
165. Koe, W.S.; Chong, W.C.; Pang, Y.L.; Koo, C.H.; Ebrahim, M.; Mohammad, A.W. Novel nitrogen and sulphur co-doped carbon quantum dots/titanium oxide photocatalytic membrane for in-situ degradation and removal of pharmaceutical compound. *J. Water Process Eng.* **2020**, *33*, 101068. [CrossRef]
166. Espındola, C.; Szymański, K.; Cristóvão, R.O.; Mendes, A.; Vilar, V.J.P.; Mozia, S. Performance of hybrid systems coupling advanced oxidation processes and ultrafiltration for oxytetracycline removal. *Catal Today* **2019**, *328*, 274–280. [CrossRef]
167. Pastrana-Martinez, L.M.; Morales-Torres, S.; Figueiredo, J.L.; Faria, J.L.; Silva, A.M. Graphene oxide based ultrafiltration membranes for photocatalytic degradation of organic pollutants in salty water. *Water Res.* **2015**, *77*, 179–190. [CrossRef]
168. Chakraborty, S.; Loutatidou, S.; Palmisano, G.; Kujawa, J.; Mavukkandy, M.O.; Al-Gharabli, S.; Curcio, E.; Arafat, H.A. Photocatalytic hollow fiber membranes for the degradation of pharmaceutical compounds in wastewater. *J. Environ. Chem. Eng.* **2017**, *5*, 5014–5024. [CrossRef]

169. Sarasidis, V.C.; Plakas, K.V.; Patsios, S.I.; Karabelas, A.J. Investigation of diclofenac degradation in a continuous photo-catalytic membrane reactor. Influence of operating parameters. *Chem. Eng. J.* **2014**, *239*, 299–311. [CrossRef]
170. Fischer, K.; Grimm, M.; Meyers, J.; Dietrich, C.; Gläser, R.; Schulze, A. Photoactive microfiltration membranes via directed synthesis of TiO_2 nanoparticles on the polymer surface for removal of drugs from water. *J. Membr. Sci.* **2015**, *478*, 49–57. [CrossRef]
171. Darowna, D.; Grondzewska, S.; Morawski, A.W.; Mozia, S. Removal of non-steroidal anti-inflammatory drugs from primary and secondary effluents in a photocatalytic membrane reactor. *J. Chem. Technol. Biotechnol.* **2014**, *89*, 1265–1273. [CrossRef]
172. Molinari, R.; Pirillo, F.; Loddo, V.; Palmisano, L. Heterogeneous photocatalytic degradation of pharmaceuticals in water by using polycrystalline TiO_2 and a nanofiltration membrane reactor. *Catal. Today* **2006**, *118*, 205–213. [CrossRef]
173. Li, W.; Li, B.; Meng, M.; Cui, Y.; Wu, Y.; Zhang, Y.; Dong, H.; Feng, Y. Bimetallic Au/Ag decorated TiO_2 nanocomposite membrane for enhanced photocatalytic degradation of tetracycline and bactericidal efficiency. *Appl. Surf. Sci.* **2019**, *487*, 1008–1017. [CrossRef]
174. Plakas, K.V.; Sarasidis, V.C.; Patsios, S.I.; Lambropoulou, D.A.; Karabelas, A.J. Novel pilot scale continuous photocatalytic membrane reactor for removal of organic micropollutants from water. *Chem. Eng. J.* **2016**, *304*, 335–343. [CrossRef]
175. Wang, C.; Wu, Y.; Lu, J.; Zhao, J.; Cui, J.; Wu, X.; Yan, Y.; Huo, P. Bioinspired synthesis of photocatalytic nanocomposite membranes based on synergy of Au-TiO_2 and polydopamine for degradation of tetracycline under visible light. *ACS Appl. Mater. Interfaces* **2017**, *9*, 23687–23697. [CrossRef]
176. Boopathy, G.; Gangasalam, A.; Mahalingam, A. Photocatalytic removal of organic pollutants and self-cleaning performance of PES membrane incorporated sulfonated graphene oxide/ZnO nanocomposite. *J. Chem. Technol. Biotechnol.* **2020**, *95*, 3012–3023. [CrossRef]
177. Zakeritabar, S.F.; Jahanshahi, M.; Peyravi, M. Photocatalytic behavior of induced membrane by ZrO_2–SnO_2 nanocomposite for pharmaceutical wastewater treatment. *Catal. Lett.* **2018**, *148*, 882–893. [CrossRef]
178. Gao, B.; Chen, W.; Liu, J.; An, J.; Wang, L.; Zhu, Y.; Sillanpää, M. Continuous removal of tetracycline in a photocatalytic membrane reactor (PMR) with $ZnIn_2S_4$ as adsorption and photocatalytic coating layer on PVDF membrane. *J. Photochem. Photobiol. A Chem.* **2018**, *364*, 732–739. [CrossRef]
179. Horovitz, I.; Avisar, D.; Baker, M.A.; Grilli, R.; Lozzi, L.; Di Camillo, D.; Mamane, H. Carbamazepine degradation using a N-doped TiO_2 coated photocatalytic membrane reactor: Influence of physical parameters. *J. Hazard. Mater.* **2016**, *310*, 98–107. [CrossRef] [PubMed]
180. Dzinun, H.; Ichikawa, Y.; Mitsuhiro, H.; Zhang, Q. Efficient immobilised TiO_2 in polyvinylidene fluoride (PVDF) membrane for photocatalytic degradation of methylene blue. *J. Membr. Sci. Res.* **2020**, *6*, 188–195.
181. Kolesnyk, I.; Kujawa, J.; Bubela, H.; Konovalova, V.; Burban, A.; Cyganiuk, A.; Kujawski, W. Photocatalytic properties of PVDF membranes modified with g-C_3N_4 in the process of Rhodamines decomposition. *Sep. Purif. Technol.* **2020**, *250*, 117231. [CrossRef]
182. Ma, N.; Zhang, Y.; Quan, X.; Fan, X.; Zhao, H. Performing a microfiltration integrated with photocatalysis using an Ag-TiO_2/HAP/Al_2O_3 composite membrane for water treatment: Evaluating effectiveness for humic acid removal and anti-fouling properties. *Water Res.* **2010**, *44*, 6104–6114. [CrossRef] [PubMed]
183. Rani, C.N.; Karthikeyan, S. Investigation of Naphthalene Removal from Aqueous Solutions in an Integrated Slurry Photocatalytic Membrane Reactor: Effect of Operating Parameters, Identification of Intermediates, and Response Surface Approach. *Polycycl. Aromat. Compd.* **2021**, *41*, 805–824. [CrossRef]
184. Moslehyani, A.; Ismail, A.; Othman, M.; Matsuura, T. Hydrocarbon degradation and separation of bilge water via a novel TiO_2-HNTs/PVDF-based photocatalytic membrane reactor (PMR). *RSC Adv.* **2015**, *5*, 14147–14155. [CrossRef]
185. Goei, R.; Lim, T.-T. Ag-decorated TiO_2 photocatalytic membrane with hierarchical architecture: Photocatalytic and anti-bacterial activities. *Water Res.* **2014**, *59*, 207–218. [CrossRef]
186. Kazemi, M.; Jahanshahi, M.; Peyravi, M. Chitosan-sodium alginate multilayer membrane developed by Fe0@ WO_3 nanoparticles: Photocatalytic removal of hexavalent chromium. *Carbohydr. Polym.* **2018**, *198*, 164–174. [CrossRef]
187. Tran, M.L.; Fu, C.-C.; Chiang, L.-Y.; Hsieh, C.-T.; Liu, S.-H.; Juang, R.-S. Immobilization of TiO_2 and TiO_2-GO hybrids onto the surface of acrylic acid-grafted polymeric membranes for pollutant removal: Analysis of photocatalytic activity. *J. Environ. Chem. Eng.* **2020**, *8*, 104422. [CrossRef]
188. Shi, Y.; Wan, D.; Huang, J.; Liu, Y.; Li, J. Stable LBL self-assembly coating porous membrane with 3D heterostructure for enhanced water treatment under visible light irradiation. *Chemosphere* **2020**, *252*, 126581. [CrossRef] [PubMed]
189. Vatanpour, V.; Karami, A.; Sheydaei, M. Central composite design optimization of Rhodamine B degradation using TiO_2 nanoparticles/UV/PVDF process in continuous submerged membrane photoreactor. *Chem. Eng. Process. Process Intensif.* **2017**, *116*, 68–75. [CrossRef]
190. Kuvarega, A.T.; Khumalo, N.; Dlamini, D.; Mamba, B.B. Polysulfone/N, Pd co-doped TiO_2 composite membranes for photocatalytic dye degradation. *Sep. Purif. Technol.* **2018**, *191*, 122–133. [CrossRef]
191. Wang, X.; Wang, G.; Chen, S.; Fan, X.; Quan, X.; Yu, H. Integration of membrane filtration and photoelectrocatalysis on g-C_3N_4/CNTs/Al_2O_3 membrane with visible-light response for enhanced water treatment. *J. Membr. Sci.* **2017**, *541*, 153–161. [CrossRef]
192. Berger, T.; Regmi, C.; Schäfer, A.; Richards, B. Photocatalytic degradation of organic dye via atomic layer deposited TiO_2 on ceramic membranes in single-pass flow-through operation. *J. Membr. Sci.* **2020**, *604*, 118015. [CrossRef]

193. Zhao, G.; Zou, J.; Chen, X.; Zhang, T.; Yu, J.; Zhou, S.; Li, C.; Jiao, F. Integration of Microfiltration and Visible-Light-Driven Photocatalysis on a $ZnWO_4$ Nanoparticle/Nickel–Aluminum-Layered Double Hydroxide Membrane for Enhanced Water Purification. *Ind. Eng. Chem. Res.* **2020**, *59*, 6479–6487. [CrossRef]
194. Gao, M.; Feng, J.; He, F.; Zeng, W.; Wang, X.; Ren, Y.; Wei, T. Carbon microspheres work as an electron bridge for degrading high concentration MB in $CoFe_2O_4$@ carbon microsphere/g-C_3N_4 with a hierarchical sandwich-structure. *Appl. Surf. Sci.* **2020**, *507*, 145167. [CrossRef]
195. Gupta, A.; Pandey, O. NbC/C heterojunction for efficient photodegradation of methylene blue under visible irradiation. *Sol. Energy* **2019**, *183*, 398–409. [CrossRef]
196. Wang, M.; Zhang, Y.; Yu, G.; Zhao, J.; Chen, X.; Yan, F.; Li, J.; Yin, Z.; He, B. Monolayer porphyrin assembled SPSf/PES membrane reactor for degradation of dyes under visible light irradiation coupling with continuous filtration. *J. Taiwan Inst. Chem. Eng.* **2020**, *109*, 62–70. [CrossRef]
197. Yu, Z.; Zeng, H.; Min, X.; Zhu, X. High-performance composite photocatalytic membrane based on titanium dioxide nanowire/graphene oxide for water treatment. *J. Appl. Polym. Sci.* **2020**, *137*, 48488. [CrossRef]
198. Salim, N.E.; Nor, N.; Jaafar, J.; Ismail, A.; Qtaishat, M.; Matsuura, T.; Othman, M.; Rahman, M.A.; Aziz, F.; Yusof, N. Effects of hydrophilic surface macromolecule modifier loading on PES/Og-C_3N_4 hybrid photocatalytic membrane for phenol removal. *Appl. Surf. Sci.* **2019**, *465*, 180–191. [CrossRef]
199. Ashar, A.; Bhatti, I.A.; Ashraf, M.; Tahir, A.A.; Aziz, H.; Yousuf, M.; Ahmad, M.; Mohsin, M.; Bhutta, Z.A. Fe^{3+}@ ZnO/polyester based solar photocatalytic membrane reactor for abatement of RB5 dye. *J. Clean. Prod.* **2020**, *246*, 119010. [CrossRef]
200. Yang, C.; Han, N.; Zhang, W.; Wang, W.; Li, W.; Xia, B.; Han, C.; Cui, Z.; Zhang, X. Adhesive-free in situ synthesis of a coral-like titanium dioxide@ poly (phenylene sulfide) microporous membrane for visible-light photocatalysis. *Chem. Eng. J.* **2019**, *374*, 1382–1393.
201. Wang, M.; Yang, G.; Jin, P.; Tang, H.; Wang, H.; Chen, Y. Highly hydrophilic poly (vinylidene fluoride)/meso-titania hybrid mesoporous membrane for photocatalytic membrane reactor in water. *Sci. Rep.* **2016**, *6*, 19148. [CrossRef] [PubMed]
202. Zhang, R.; Cai, Y.; Zhu, X.; Han, Q.; Zhang, T.; Liu, Y.; Li, Y.; Wang, A. A novel photocatalytic membrane decorated with PDA/RGO/Ag_3PO_4 for catalytic dye decomposition. *Colloids Surf. A Physicochem. Eng. Asp.* **2019**, *563*, 68–76. [CrossRef]
203. Wang, X.; Shi, F.; Huang, W.; Fan, C. Synthesis of high quality TiO_2 membranes on alumina supports and their photocatalytic activity. *Thin Solid Film.* **2012**, *520*, 2488–2492. [CrossRef]
204. Wu, X.-Q.; Shen, J.-S.; Zhao, F.; Shao, Z.-D.; Zhong, L.-B.; Zheng, Y.-M. Flexible electrospun MWCNTs/Ag_3PO_4/PAN ternary composite fiber membranes with enhanced photocatalytic activity and stability under visible-light irradiation. *J. Mater. Sci.* **2018**, *53*, 10147–10159. [CrossRef]
205. Yu, Z.; Min, X.; Li, F.; Yin, D.; Peng, Y.; Zeng, G. A mussel-inspired method to fabricate a novel reduced graphene oxide/$Bi_{12}O_{17}Cl_2$ composites membrane for catalytic degradation and oil/water separation. *Polym. Adv. Technol.* **2019**, *30*, 101–109. [CrossRef]
206. Daels, N.; Radoicic, M.; Radetic, M.; Van Hulle, S.W.; De Clerck, K. Functionalisation of electrospun polymer nanofibre membranes with TiO_2 nanoparticles in view of dissolved organic matter photodegradation. *Sep. Purif. Technol.* **2014**, *133*, 282–290. [CrossRef]
207. Fischer, K.; Gläser, R.; Schulze, A. Nanoneedle and nanotubular titanium dioxide–PES mixed matrix membrane for photocatalysis. *Appl. Catal. B Environ.* **2014**, *160*, 456–464. [CrossRef]
208. Ong, C.B.; Mohammad, A.W.; Ng, L.Y. Integrated adsorption-solar photocatalytic membrane reactor for degradation of hazardous Congo red using Fe-doped ZnO and Fe-doped ZnO/rGO nanocomposites. *Environ. Sci. Pollut. Res.* **2019**, *26*, 33856–33869. [CrossRef] [PubMed]
209. Alyarnezhad, S.; Marino, T.; Parsa, J.B.; Galiano, F.; Ursino, C.; Garcìa, H.; Puche, M.; Figoli, A. Polyvinylidene fluoride-graphene oxide membranes for dye removal under visible light irradiation. *Polymers* **2020**, *12*, 1509. [CrossRef]
210. Lyubimenko, R.; Busko, D.; Richards, B.S.; Schäfer, A.I.; Turshatov, A. Efficient photocatalytic removal of methylene blue using a metalloporphyrin–poly (vinylidene fluoride) hybrid membrane in a flow-through reactor. *ACS Appl. Mater. Interfaces* **2019**, *11*, 31763–31776. [CrossRef]
211. Zhao, H.; Chen, S.; Quan, X.; Yu, H.; Zhao, H. Integration of microfiltration and visible-light-driven photocatalysis on g-C_3N_4 nanosheet/reduced graphene oxide membrane for enhanced water treatment. *Appl. Catal. B Environ.* **2016**, *194*, 134–140. [CrossRef]
212. Xu, H.; Ding, M.; Chen, W.; Li, Y.; Wang, K. Nitrogen–doped GO/TiO_2 nanocomposite ultrafiltration membranes for improved photocatalytic performance. *Sep. Purif. Technol.* **2018**, *195*, 70–82. [CrossRef]
213. Laohaprapanon, S.; Vanderlipe, A.D.; Doma, B.T., Jr.; You, S.-J. Self-cleaning and antifouling properties of plasma-grafted poly (vinylidene fluoride) membrane coated with ZnO for water treatment. *J. Taiwan Inst. Chem. Eng.* **2017**, *70*, 15–22. [CrossRef]
214. Li, B.; Chu, J.; Li, Y.; Meng, M.; Cui, Y.; Li, Q.; Feng, Y. Preparation and Performance of Visible-Light-Driven Bi_2O_3/ZnS Heterojunction Functionalized Porous CA Membranes for Effective Degradation of Rhodamine B. *Phys. Status Solidi (A)* **2018**, *215*, 1701061. [CrossRef]
215. Bai, H.; Zan, X.; Juay, J.; Sun, D.D. Hierarchical heteroarchitectures functionalized membrane for high efficient water purification. *J. Membr. Sci.* **2015**, *475*, 245–251. [CrossRef]
216. Rani, C.N.; Karthikeyan, S. Feasibility study of acenaphthene degradation in a novel slurry UV photocatalytic membrane reactor: Effect of operating parameters and optimization using response surface modeling. *Chem. Eng. Process.-Process Intensif.* **2020**, *155*, 108051. [CrossRef]

217. Nascimben Santos, E.; Agoston, A.; Kertész, S.; Hodúr, C.; László, Z.; Pap, Z.; Kása, Z.; Alapi, T.; Krishnan, S.G.; Arthanareeswaran, G. Investigation of the applicability of TiO_2, $BiVO_4$, and WO_3 nanomaterials for advanced photocatalytic membranes used for oil-in-water emulsion separation. *Asia-Pac. J. Chem. Eng.* **2020**, *15*, e2549. [CrossRef]
218. Zhou, J.; Zhao, Z.; Wang, Y.; Ding, Z.; Xu, X.; Peng, W.; Fan, J.; Zhou, X.; Liu, J. $BiOCl_{0.875}Br_{0.125}$/polydopamine functionalized PVDF membrane for highly efficient visible-light-driven photocatalytic degradation of roxarsone and simultaneous arsenic immobilization. *Chem. Eng. J.* **2020**, *402*, 126048. [CrossRef]
219. Gao, Y.; Yan, N.; Jiang, C.; Xu, C.; Yu, S.; Liang, P.; Zhang, X.; Liang, S.; Huang, X. Filtration-enhanced highly efficient photocatalytic degradation with a novel electrospun rGO@ TiO_2 nanofibrous membrane: Implication for improving photocatalytic efficiency. *Appl. Catal. B Environ.* **2020**, *268*, 118737. [CrossRef]
220. Shareef, U.; Othman, M.H.D.; Ismail, A.F.; Jilani, A. Facile removal of bisphenol A from water through novel Ag-doped TiO_2 photocatalytic hollow fiber ceramic membrane. *J. Aust. Ceram. Soc.* **2020**, *56*, 29–39. [CrossRef]
221. Lin, Y.-C.; Wang, D.K.; Liu, J.-Y.; Niaei, A.; Tseng, H.-H. Low band-gap energy photocatalytic membrane based on $SrTiO_3$–Cr and PVDF substrate: BSA protein degradation and separation application. *J. Membr. Sci.* **2019**, *586*, 326–337. [CrossRef]
222. Shi, Y.; Huang, J.; Zeng, G.; Cheng, W.; Hu, J.; Shi, L.; Yi, K. Evaluation of self-cleaning performance of the modified g-C_3N_4 and GO based PVDF membrane toward oil-in-water separation under visible-light. *Chemosphere* **2019**, *230*, 40–50. [CrossRef]
223. Leong, S.; Low, Z.X.; Liu, Q.; Hapgood, K.; Zhang, X.; Wang, H. Preparation of supported photocatalytic membrane from mesoporous titania spheres for humic acid removal from wastewater. *Asia-Pac. J. Chem. Eng.* **2016**, *11*, 611–619. [CrossRef]
224. Golshenas, A.; Sadeghian, Z.; Ashrafizadeh, S.N. Performance evaluation of a ceramic-based photocatalytic membrane reactor for treatment of oily wastewater. *J. Water Process Eng.* **2020**, *36*, 101186. [CrossRef]
225. Xu, H.; Li, Y.; Ding, M.; Chen, W.; Wang, K.; Lu, C. Engineered photocatalytic material membrane assemblies for removing nitrate from water. *ACS Sustain. Chem. Eng.* **2018**, *6*, 7042–7051. [CrossRef]
226. Ong, C.; Lau, W.; Goh, P.; Ng, B.; Ismail, A. Investigation of submerged membrane photocatalytic reactor (sMPR) operating parameters during oily wastewater treatment process. *Desalination* **2014**, *353*, 48–56. [CrossRef]
227. Xu, Z.; Wu, T.; Shi, J.; Teng, K.; Wang, W.; Ma, M.; Li, J.; Qian, X.; Li, C.; Fan, J. Photocatalytic antifouling PVDF ultrafiltration membranes based on synergy of graphene oxide and TiO_2 for water treatment. *J. Membr. Sci.* **2016**, *520*, 281–293. [CrossRef]
228. Mungondori, H.H.; Tichagwa, L.; Katwire, D.M.; Aoyi, O. Preparation of photo-catalytic copolymer grafted asymmetric membranes (N-TiO_2-PMAA-g-PVDF/PAN) and their application on the degradation of bentazon in water. *Iran. Polym. J.* **2016**, *25*, 135–144. [CrossRef]
229. Lin, H.; Zhang, M.; Wang, F.; Meng, F.; Liao, B.-Q.; Hong, H.; Chen, J.; Gao, W. A critical review of extracellular polymeric substances (EPSs) in membrane bioreactors: Characteristics, roles in membrane fouling and control strategies. *J. Membr. Sci.* **2014**, *460*, 110–125. [CrossRef]
230. Zhang, W.; Hao, T. Insights into the role of concentration polarization on the membrane fouling and cleaning during the aerobic granular sludge filtration process. *Sci. Total Environ.* **2022**, *813*, 151871. [CrossRef] [PubMed]
231. Augugliaro, V.; Litter, M.; Palmisano, L.; Soria, J. The combination of heterogeneous photocatalysis with chemical and physical operations: A tool for improving the photoprocess performance. *J. Photochem. Photobiol. C Photochem. Rev.* **2006**, *7*, 127–144. [CrossRef]
232. Gao, W.; Liang, H.; Ma, J.; Han, M.; Chen, Z.-l.; Han, Z.-s.; Li, G.-b. Membrane fouling control in ultrafiltration technology for drinking water production: A review. *Desalination* **2011**, *272*, 1–8. [CrossRef]
233. Zheng, H.; Zhu, M.; Wang, D.; Zhou, Y.; Sun, X.; Jiang, S.; Li, M.; Xiao, C.; Zhang, D.; Zhang, L. Surface modification of PVDF membrane by CNC/Cu-MOF-74 for enhancing antifouling property. *Sep. Purif. Technol.* **2023**, *306*, 122599. [CrossRef]
234. Mozia, S. Photocatalytic membrane reactors (PMRs) in water and wastewater treatment. A review. *Sep. Purif. Technol.* **2010**, *73*, 71–91. [CrossRef]
235. Mendret, J.; Hatat-Fraile, M.; Rivallin, M.; Brosillon, S. Hydrophilic composite membranes for simultaneous separation and photocatalytic degradation of organic pollutants. *Sep. Purif. Technol.* **2013**, *111*, 9–19. [CrossRef]
236. Wang, P.; Fane, A.G.; Lim, T.-T. Evaluation of a submerged membrane vis-LED photoreactor (sMPR) for carbamazepine degradation and TiO_2 separation. *Chem. Eng. J.* **2013**, *215*, 240–251. [CrossRef]
237. Zhang, J.; Wang, L.; Zhang, G.; Wang, Z.; Xu, L.; Fan, Z. Influence of azo dye-TiO_2 interactions on the filtration performance in a hybrid photocatalysis/ultrafiltration process. *J. Colloid Interface Sci.* **2013**, *389*, 273–283. [CrossRef]
238. Chin, J.Y.; Ahmad, A.L.; Low, S.C. Evolution of photocatalytic membrane for antibiotics degradation: Perspectives and insights for sustainable environmental remediation. *J. Water Process Eng.* **2023**, *51*, 103342. [CrossRef]

Disclaimer/Publisher's Note: The statements, opinions and data contained in all publications are solely those of the individual author(s) and contributor(s) and not of MDPI and/or the editor(s). MDPI and/or the editor(s) disclaim responsibility for any injury to people or property resulting from any ideas, methods, instructions or products referred to in the content.